Title

The Development of Quantifiable 3-Dimensional Korean Adult Normative Skulls and Its Clinical Application

Author

Lee, Peter

Publication Date

2016

Peer reviewed|Thesis/dissertation

UNIVERSITY OF CALIFORNIA

Los Angeles

The Development of Quantifiable 3-Dimensional Korean Adult Normative Skulls and Its Clinical Application

A thesis submitted in partial satisfaction of the requirements

for the degree of Master of Science in Oral Biology

by

Peter Byung Chan Lee

2016

ABSTRACT OF THE THESIS

The Development of Quantifiable 3-Dimensional Korean Adult Normative Skulls and Its Clinical Application

by

Peter Byung Chan Lee

Master of Science in Oral Biology

University of California, Los Angeles, 2016

Professor Won Moon, Co-chair

Professor Sotirios Tetradis, Co-chair

Objectives: The establishment of a true 3-dimensional (3D) skeletal analysis of cone beam computed tomography (CBCT) images for orthodontic diagnoses has been a challenging endeavor, as previously proposed 3D analyses still rely upon 2-dimensional (2D) linear and angular measurements. In previous studies, the UCLA Section of Orthodontics, in a collaborative effort with the Laboratory of Neuro Imaging (LONI),

developed a method for surface mapping a skull in three dimensions and expressing the curved outline of the structure using geometric algebraic methods. The long-term objective of the study is to establish a true three-dimensional (3D) skeletal analysis involving quantifiable 3D subnorms with respect to age, gender, and ethnicity. The specific aim of this study is to create a quantifiable 3D Korean adult normative skull that allows superimposition and comparison.

Materials and Methods: Quantifying samples followed the inclusion criteria of Korean adult male/female of ages greater than 18 and skeletal class I relationship based on cephalometric analyses. Patients with craniofacial defects, significant skeletal asymmetry, and/or previous history of orthodontic treatment were excluded. Using 11 male and 13 female normative CBCT images, the surface map and curved outline of each skull were generated by projective mapping and harmonic interpolation, and acquisition of points along the surface, respectively. The Procrustes superimposition method was used for normalization of samples.

Results: This normalized form provided a foundation for the comparison of an individual to the average, allowing sample differences to be visualized and quantified. The establishment of a linear distance map, directional vector map, and statistical map effectively showed clear deviation of individual skulls to the norm.

Conclusion: The establishment of subnorms is a difficult task due to limited sample size from stringent inclusion and exclusion criteria, but can be successfully done utilizing the methods we developed. Further studies accounting for ethnicity, gender, and age will strengthen the diagnostic power of CBCT images in orthodontics.

The thesis of Peter Byung Chan Lee is approved.

Reubin Han-Kyu Kim

Ki-Hyuk Shin

Won Moon, Committee Co-Chair

Sotirios Tetradis, Committee Co-Chair

University of California, Los Angeles

2016

TABLE OF CONTENTS AND LISTS

1. Introduction

For almost a century, 2-dimensional (2D) radiographic cephalometric imaging has been an invaluable tool in orthodontics, allowing clinicians to evaluate the interrelationships of the skeleton, dentition, and soft tissues. With the introduction of 3-dimensional (3D) Cone Beam Ccomputed Tomography (CBCT) imaging and its continual advancement in technology, a 3D cephalometric application to improve the analysis of orthodontic patients is necessary. In order to comprehend the importance of quantifiable 3D analysis in diagnosis and treatment planning, one must first overview the history and limitations of current imaging in orthodontics.

1-1. History of Cephalometric Imaging and Analyses

Malocclusions and craniofacial anomalies can adversely affect quality of life. Orthodontic and dentofacial orthopedic treatment can address the correction of malocclusions and facial disproportions from dental and skeletal discrepancies and provide esthetic, psychosocial, and functional improvements.[1] Therefore, evaluating the interrelationship of the structural components of the human face is an essential diagnostic factor in orthodontics.[2] Traditionally, orthodontic diagnostic records consist of several key components such as clinical exam, dental study models, intraoral/extraoral photographs, radiographs, and cephalometric analysis. Although each component arguably is equally valuable, lateral cephalograms and cephalometric analyses are particularly essential, for they take into account the underlying skeletal features that must

be analyzed in order to achieve a harmonious dental/skeletal relationship and profile for patients.

Roentgenographic cephalometry was first introduced to orthodontics by Dr. Birdsall Holly Broadbent in 1931, providing the first tool to study skeletal, dental, and soft tissue structures of the craniofacial region (Figure 1).[3] The use of cephalometry expanded to include the study of craniofacial growth and development, diagnosis and treatment planning, and evaluation of treatment progress. Consequently, it provided an avenue for the development of a series of analyses.[4,5] For example, the Steiner analysis, developed by Dr. Cecil Steiner in the 1950s, can be considered the first modern cephalometric analysis. It displayed individual measurements and their interrelationship into a pattern, providing specific guidelines for the use of cephalometric measurements in treatment planning. Another example is the Sassouni analysis, which was the first analysis to emphasize both vertical and horizontal proportions. It evaluated the sagittal position of the face and the dentition by emphasizing the relationship between various points to arcs (Figure 2).[2,6]

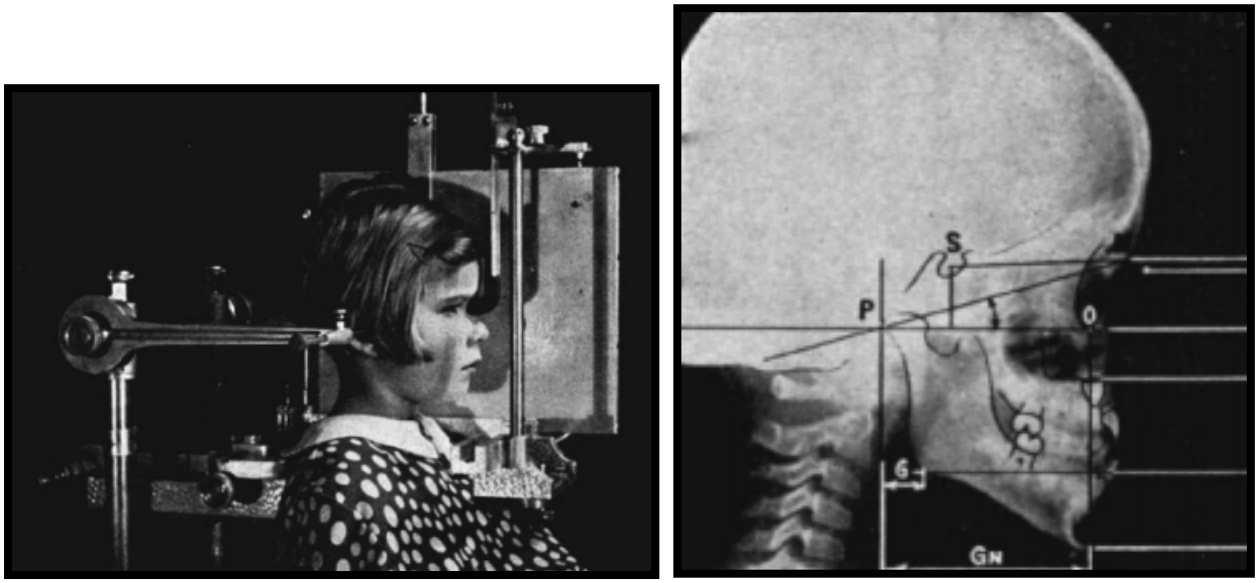

Figure 1: (Adapted from Broadbent et al)[3] The child's head adjusted to the Broadbent Head Holder for lateral roentgenogram (left). Lateral roentgenogram of a child with a developing Class III malocclusion shown with tracing of hard-tissue landmarks (right).

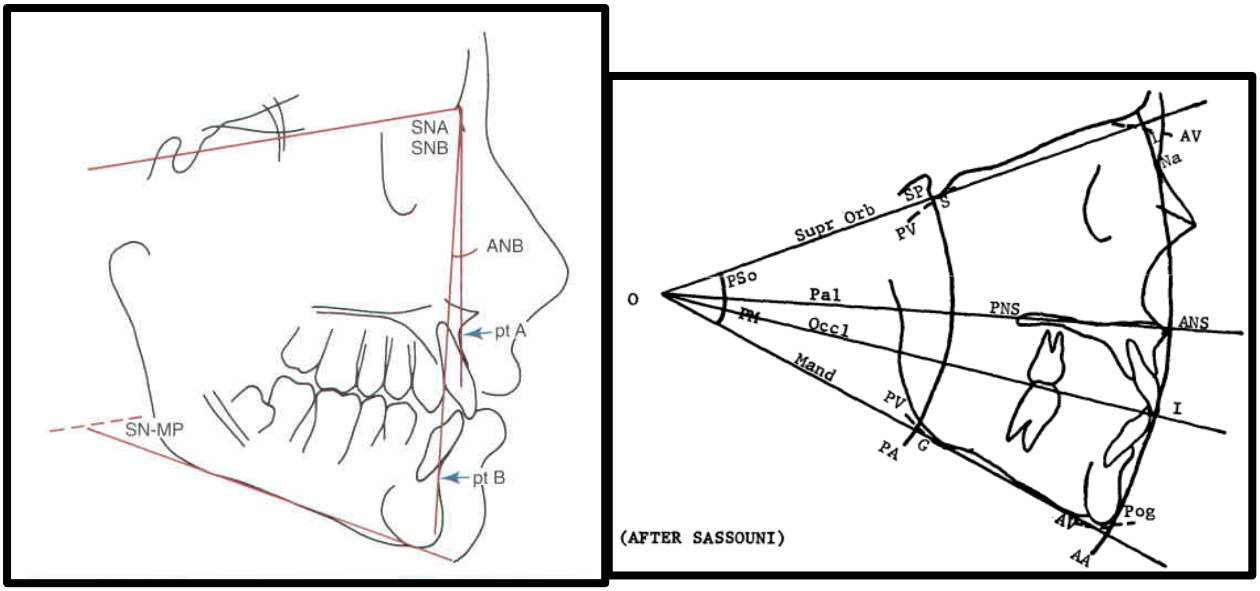

Figure 2: (Adapted from Proffit)[2] Steiner Analysis (left) showing the angles SNA and SNB to establish relationship of the maxilla and mandible to the cranial base (SN). (Adapted from Altemus et al)[6] Sassouni Analysis (right) showing the concept of proportionality in horizontal and vertical dimensions.

1-2. Limitations of Cephalometric Imaging and Analysis

Starting from the forefathers of orthodontics such as Steiner, Downs, Sassouni, Tweed, and Ricketts, there are over 50 different analyses available to clinicians today. Although these varying analyses offer a generally consistent and dependable guide to diagnosis and treatment planning, no one analysis is universally accepted to be superior over others.[4] Notably, all analyses share a major shortcoming that is inherent in conventional radiographs: 3-dimensional structures are being analyzed in 2-dimensions, relying upon 2D linear and angular measures with anthropometric and arbitrary landmarks.

The inherent limitations of cephalometric films are: [7,8]

- 2D representation of a 3D object
- Superimposition of right- and left-sided structures resulting in anatomic occlusion
- Radiographic projection error restricting true size comparison
- Operator error yielding image variability
- Landmark identification error during cephalometric analysis, decreasing reliability of cephalometrics
- Assumption that the patient does not have any skeletal asymmetry

In addition to the above-mentioned limitations, cephalometric analyses fail to objectively derive normative 2D measurements with proper consideration for age, gender, and ethnic differences; hence, they do not always offer a consistent and dependable guide to diagnosis and treatment planning. Steiner stressed that any analysis is not complete until it has been individualized and adjusted to the needs of the particular patients under consideration, as they serve only as guides for individuals.[9,10]

1-3. Introduction of Cone Beam Computed Tomography

For many years, 3D information was confined to plaster and the clinical examination of the patient until the introduction of CBCT into dentistry in 1998.[11] Since then, there has been an enormous interest in this technology and its application in the field of orthodontics. Offering an accurate volumetric 3D representation of hard and soft tissues of the skull, CBCT provided a breakthrough in the field of orthodontics, allowing clinicians to accurately see the true anatomical structures for the purpose of diagnosis and treatment planning for the first time.[12] The application of CBCT in orthodontics became limitless in all phases of the management of orthodontic patients, including diagnosis and treatment planning, assessment of treatment progress and outcomes, as well as risk assessment (Table 1).[13]

Table 1: Application of CBCT in Orthodontics

Orthodontic Situation	CBCT Application
Diagnosis	Assessment of skeletal structures and dental structures Skeletal jaw relation Symmetry/Asymmetry 3D evaluation of impacted tooth position and anatomy Pharyngeal airway analysis Assessment of TMJ complex in three dimensions Cleft palate assessment
Treatment Planning	Orthognathic surgery treatment planning in true 1:1 imaging

	Planning for placement of TADs Accurate estimation of space required for unerupted/impacted teeth
Treatment Progress	Assessment of dentofacial orthopedics Outcomes of alveolar bone grafts in cleft palate cases Orthognathic surgery superimposition
Risk Assessment	Assessment of orthodontics induced root resorption Post treatment Temporomandibular Disorder (TMD)

1-4. Advantages of CBCT over Lateral Cephalogram

Various pieces of literature advocate the use of CBCT images in orthodontics. The literature emphasize the significant advantages that 3D imaging offers over conventional 2D imaging: [12,14]

- 3D imaging produces high definition images with accurate volumetric 3D representation of hard and soft tissues of the skull.
- The images are of real size 1:1 scale and allow for the evaluation of the anatomical truth and provide accurate measurements.
- 3D imaging overcomes the limitation of overlapped anatomical structures and identifies and quantifies asymmetry.
- It allows visualization of airway abnormalities and condylar positions.

The named advantages present increased potential utility of CBCT compared to 2D cephalogram. For example, it can lead to refinement in preoperative planning for surgical procedures.[15,16] It also provides improved accuracy and diagnostic ability in

patients with marked facial asymmetry since symmetry of anatomic landmarks and an average of the two sides are not assumed in 3D imaging.[17] Furthermore, CBCT imaging offers accurate landmark identification and fine details in surface and contours, providing additional knowledge of the skeleton and dentition.[18,19]

1-5. Limitations of Current 3D Analysis

Since the introduction of CBCT, many 3D analyses have been proposed. While they overcame some flaws that were inherent with 2D conventional cephalogram, they still rely mainly on linear and angular measurements between landmarks.[20,21,22] For example, Cho et al utilized similar skeletal and dental landmarks previously established in 2D analyses with additional new landmarks and reference planes (Figure 3). While the coordinate system consisting of three axes (x, y, and z) with their origin at Nasion (0, 0, 0) is employed, the analysis still relies heavily upon linear and angular measurements with identified landmarks.[20]

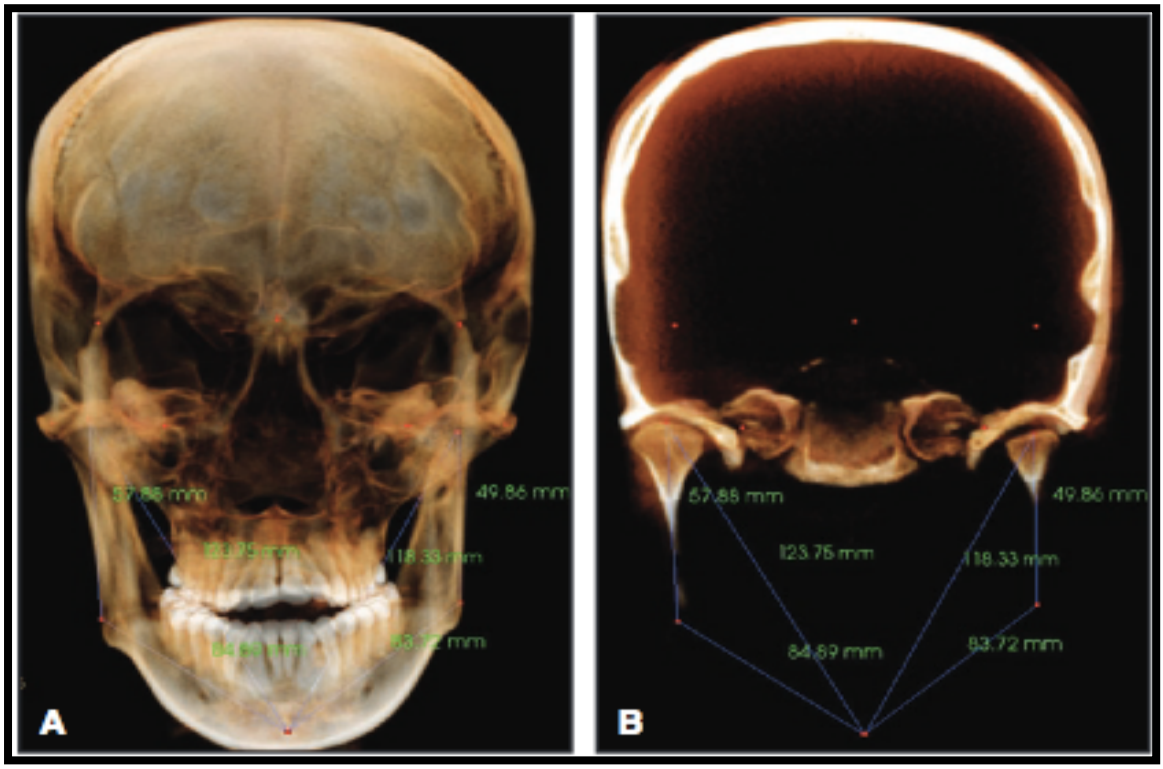

Figure 3: A and B illustrate mandibular asymmetry with right and left ramal height and body length. Mandibular length is measured from the middle of the superior surface of condylar head to pogonion. It utilizes landmarks with 2D linear measures to describe 3D asymmetry.

In another 3D study, Bayome et al[22] advanced the previous 3D analyses by evaluating the curved nature of the mandible and maxilla, although still utilizing 35 landmarks (Figure 4). The study stressed deeper understanding of mathematics in order to understand this proposed 3D analysis.[22]

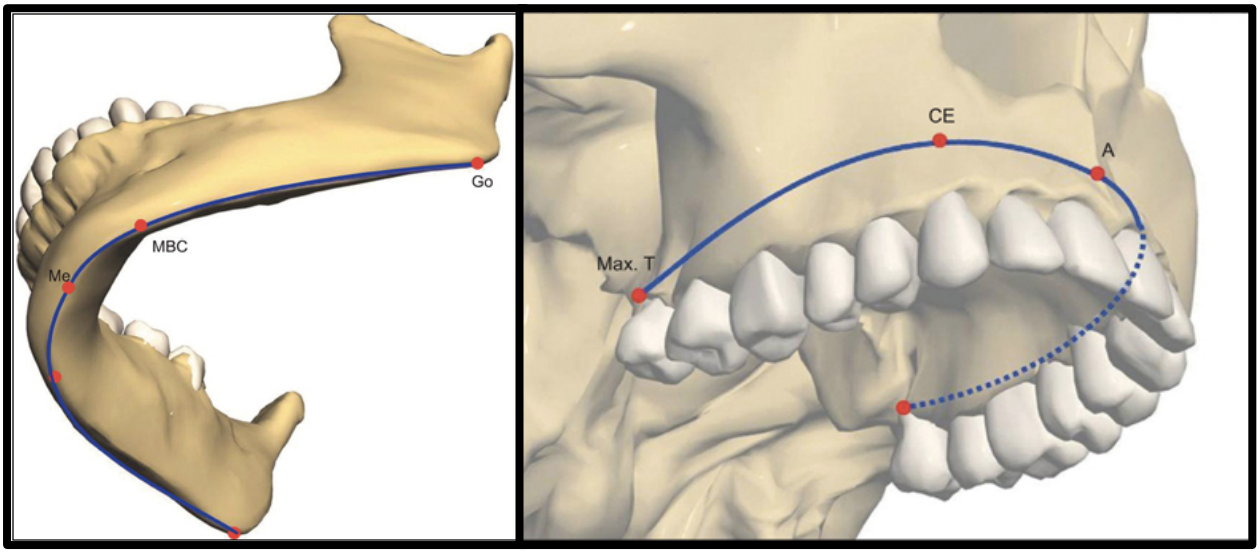

Figure 4: Mandibular and Maxillary basal curve length. The approximation of the curvature is calculated using the 4th-degree polynomial equation f(x).

While these and other proposed 3D analyses contribute to efforts in utilizing 3D imaging in diagnosis and treatment planning, it is important to recognize that limitations still do exist and many proposed 3D analyses do not give us the comprehensive anatomic truth that we are seeking to analyze in three dimensions.

1-6. Preliminary Studies and Innovation of 3D Analysis

The Section of Orthodontics at University of California Los Angeles (UCLA) School of Dentistry has an ongoing 3D analysis project under the Principal Investigator, Dr. Won Moon. The project has shown great progress from residents' contribution and collaboration with Dr. Boris Gutman from the Laboratory of Neuro Imaging (LONI). In a recent study by Dr. Ryan McComb, a method of describing the topological characteristics of the skull using surface meshes was successfully developed. 67 CBCT images were used, and the extracted mesh structures were registered using a method

called patch-matching algorithm. An average surface structure of the group was created using 7-parameter Procrustes alignment (Figure 5).[23] The same Procrustes method was then utilized to superimpose a sample on the average and colorized displacement maps were established for evaluation (Figure 6).

Figure 5: (Image adapted from McComb)[23] 67 skull average (clockwise from top left) in right lateral, frontal, left lateral, bottom up, posterior, and top down views. The average displays a smooth, harmonious skull model.

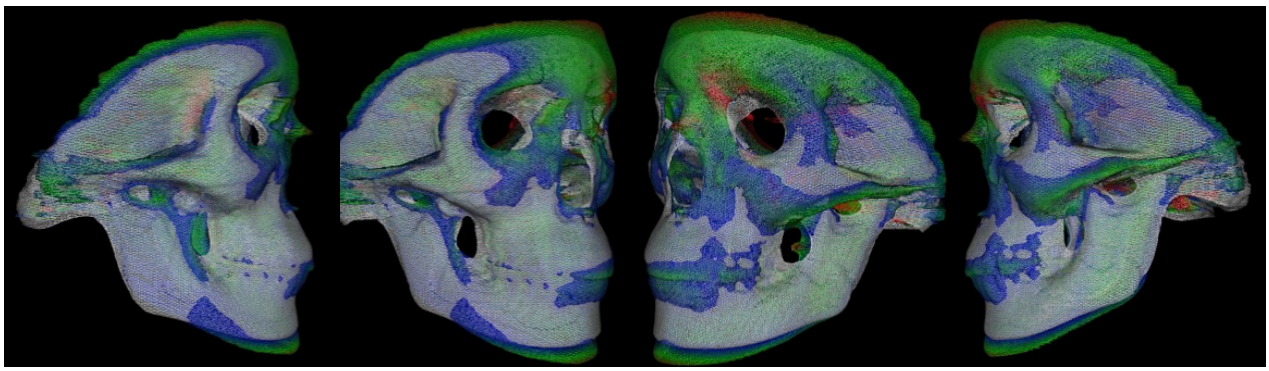

Figure 6: (Image adapted from McComb)[23] Colorized displacement map of a subject superimposed to the 67 skull average.

In studies by Drs. Rena Khullar, Thais Soares, and Jay Sung, the outline of the skull was successfully demonstrated by a 3D curve using Fourier descriptors. Dr. Khullar utilized 104 points along the border of the mandible and applied elliptical Fourier functions to describe the image (Figure 7).[24] This successful result allowed further studies by Drs. Soares and Sung to establish the entire craniofacial structure represented by curved outlines (Figure 8).[25] The Procrustes alignment method was also employed as the method of superimposition that allows size standardization and best fit for comparison along three axes (Figure 9).

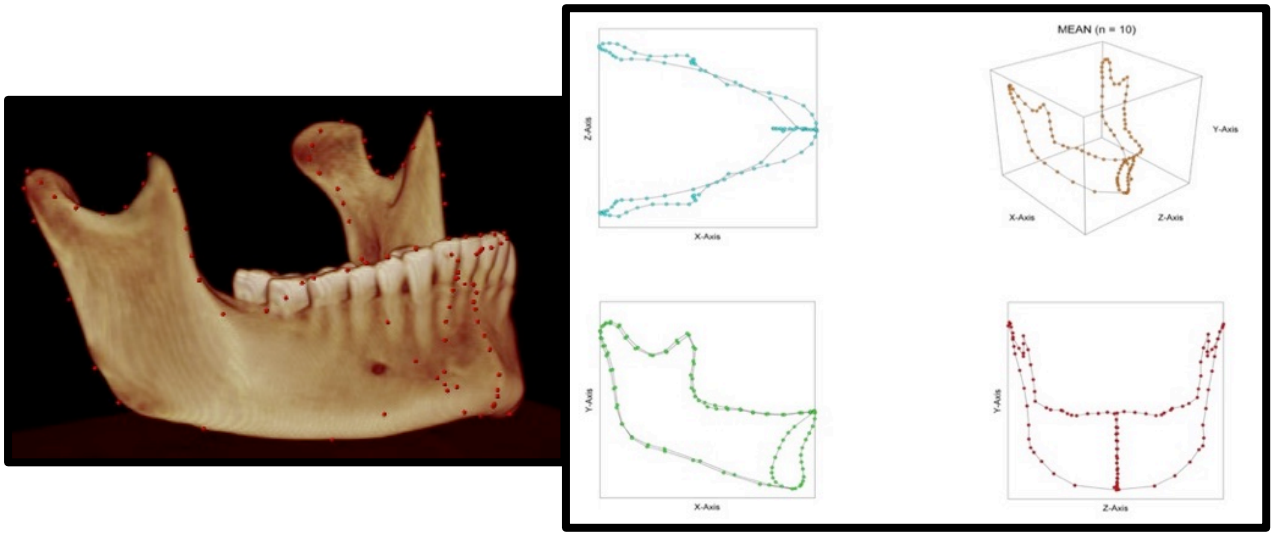

Figure 7: (Image adapted from Khullar et al.)[24] Outline of mandible (left). Boundary outline of mandible based on the mean data (n=10), in xz, xy, yz, and xyz views.

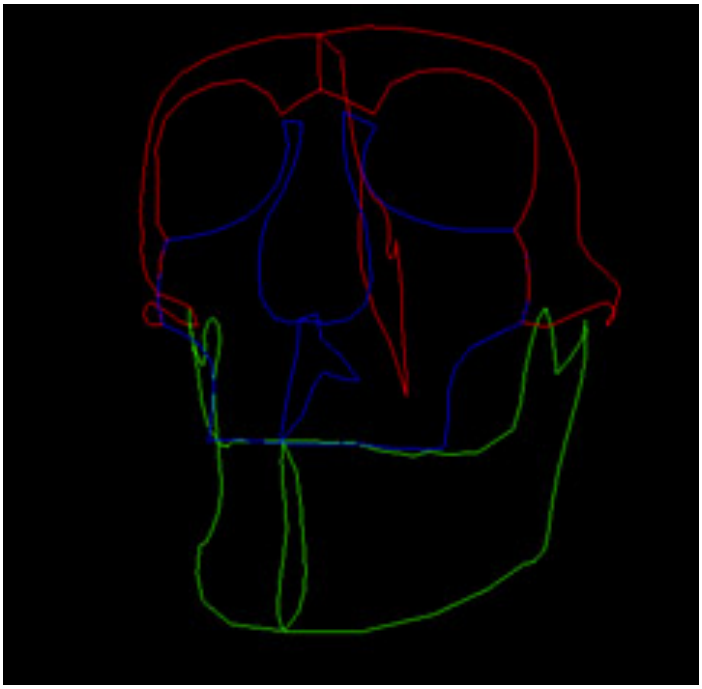

Figure 8: (Image adapted from Sung)[25] The average craniofacial complex of 10 patients established by applying the invert transformation and repositioning each component (cranial base/zygoma, maxilla, and mandible) with respect to one another.

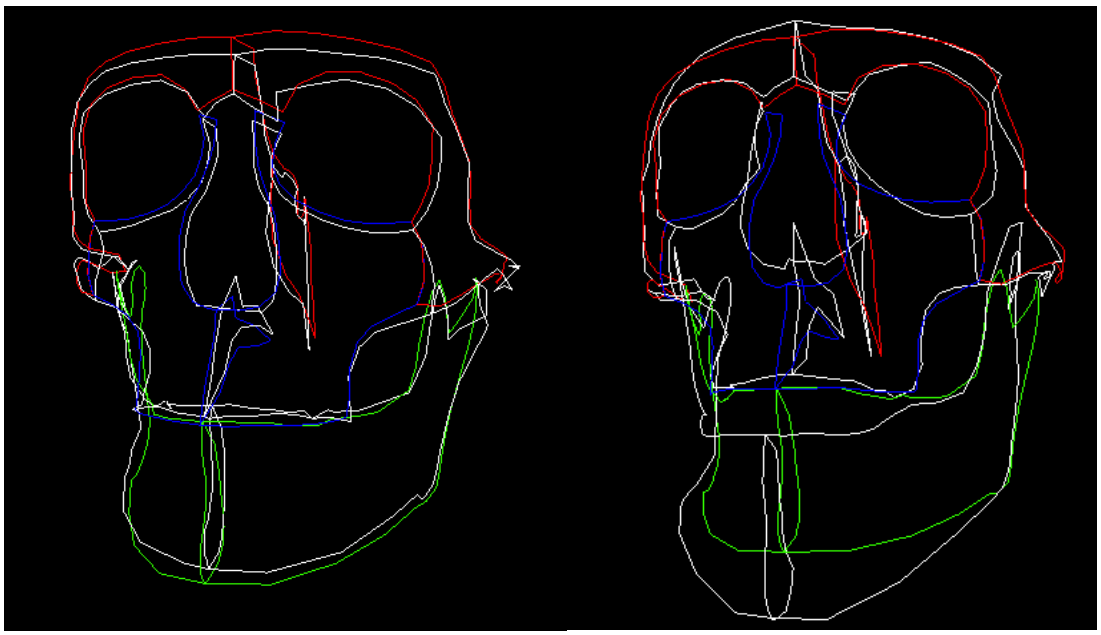

Figure 9 (Image adapted from Sung)[25] An internal sample superimposed to the 10 sample average (left). An abnormal sample superimposed to the average (right).

The Laboratory of Neuroimaging (LONI) at UCLA, our collaborator in this research project, developed a pipeline that assists in processing the 3D craniofacial image information towards producing an average skull shape. This study will be the first to establish true 3D norms and will allow future investigation for further normative data with respect to other specific ethnic, gender, and age groups.

1-7. Aims of the Study

This study seeks to find quantifiable 3D norms that can finalize a 3D cephalometric analysis by aiming to:

1) Establish quantifiable 3D sub-norms of the Korean adult skull based on gender. In an effort to accomplish this, mapping the surface of the skull with a triangular

mesh approach and representing the curved outline with Fourier descriptors will be employed.

2) Develop colorized displacement, vector, and statistical maps for improved analysis of superimposition of an individual to the respective sub-norm. The Procrustes superimposition method will be employed.

This innovative method will provide the ability to consider morphological characteristics of a patient's skull anatomy and easily visualize such differences with respect to the sub-norm.

2. Materials and Methods

This project, with the help of technical tools developed by LONI, applied the methods used in previous studies on surface mapping and curve analysis of the mandible, maxilla, and cranial base. On a broad level, the technical protocol for the project is summarized below, and described in more detail in this section (Figure 10).

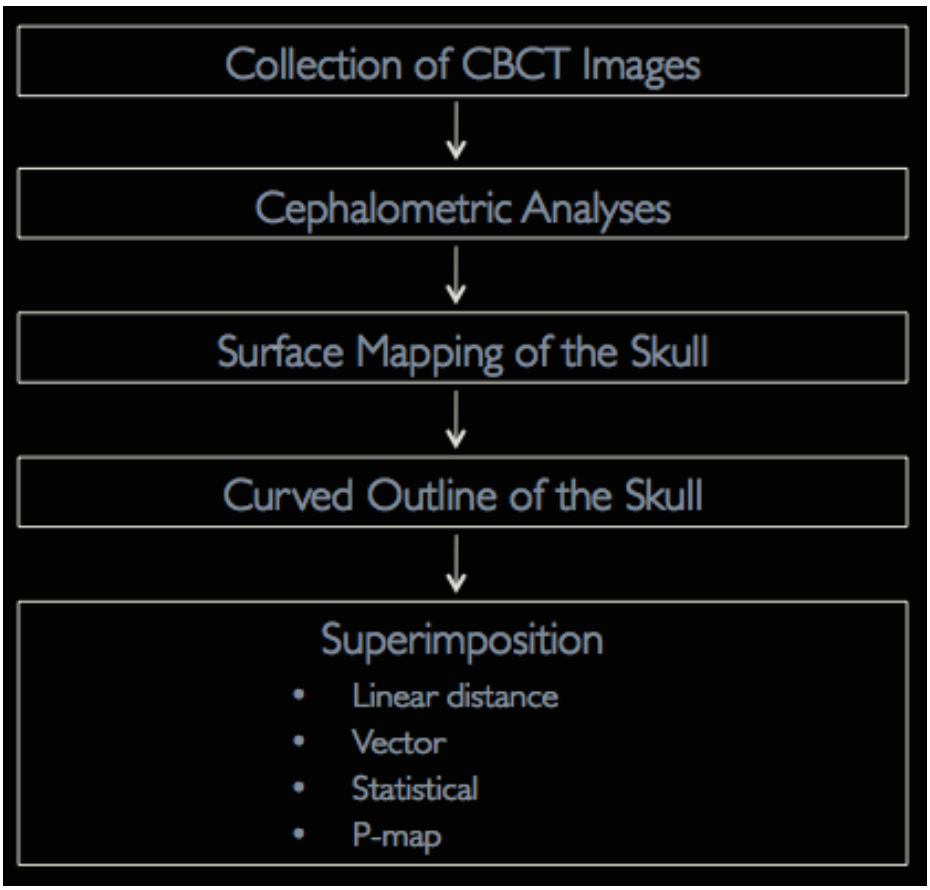

Figure 10: Diagram illustrating the workflow involved from data collection to 3D subnorm creation and superimposition.

2-1. Collection of CBCT Images

CBCT images of candidates for orthodontic treatment taken at the Department of Orthodontics, Kyung Hee University with the Alphard 3030 Model 3D X-ray CT Scanner were collected and reviewed. Images were uploaded into the Dolphin Imaging ® 11.5 Software for initial analysis to exclude any patients with significant craniofacial defects and gross skeletal asymmetry. To determine the skeletal class I relationship and mesocephalic pattern of samples as shown in Table 2, cephalometric analyses were performed.

Inclusion Criteria	➢ Skeletal class I relationship (See 2. Cephalometric Analyses below) ➢ Mesocephalic pattern ➢ Age from 18 and above
Exclusion Criteria	➢ Significant craniofacial defects (i.e. cleft palate, cleft lip, etc) ➢ Gross skeletal asymmetry or deformity ➢ History of orthodontic treatment ➢ History of orthognathic or plastic surgery

Table 2: Inclusion and exclusion criteria used for sample selection

2-2. Cephalometric Analyses

After initial screening of samples for significant craniofacial defects or gross skeletal deformity, 2D cephalograms from 3D scans were generated for all the qualifying samples and digitally traced prior to generating cephalometric analyses. In determining skeletal class I relationship and mesocephalic pattern for candidates, three cephalometric analyses – Steiner & Wits, Ricketts, and Sassouni – were generated and examined on Dolphin Imaging ® 11.5 Software. Following examination, 11 Korean adult male samples (KM) between age 18 and 36, and 13 Korean adult female samples (KF) between age 18 and 51 were qualified to be included in the study (Table 3). The ANB value ranged from -0.1 to 3.6 for KM and 0.1 to 3.9 for KF while Wits ranged from -4 to 1.4 for KM and -5.7 to 4.7 for KF. Convexity ranged from -1.2 to 5.1 for KM and -0.9 to 3.9 for KF. Lastly, MP-SN ranged from 25.2 to 36.4 for KM and 27.2 to 38.6 for KF. Although some of the values for certain patients were slightly above one standard deviation, we used clinical judgment to include them in our study.

Table 3: ANB, Wits and Convexity values for male/female samples

	Age at CBCT	ANB	Wits	Convexity	MP-SN
KM001	25Y7M	-0.1	-2.7	-0.7	31.5
KM002	18Y9M	2.5	-3.0	3.7	25.2
KM003	23Y6M	2.1	-4	1.0	25.5
KM004	24Y2M	0.1	-2.5	-0.8	29.9
KM005	25Y4M	1.9	0.5	1.0	28.6
KM007	28Y7M	2.3	-3.9	1.7	25.3
KM008	28Y1M	3.2	-0.2	3.7	32.4
KM009	36Y9M	0.2	-2.7	-1.1	33.6
KM011	27Y7M	3.6	-0.7	5.1	28.2
KM012	20Y	1.2	-0.6	-1.2	36.4
KM013	21Y	3.1	1.4	4.5	29.5
KF001	35Y3M	2.8	-0.1	2.8	29.7
KF002	22Y6M	2.6	-1.4	1.8	30.4
KF003	26Y5M	0.1	-2.8	-0.9	30.1
KF004	26Y	2.7	-4.2	3.1	38.6
KF005	36Y4M	2.6	4.7	1.9	30.0
KF006	21Y	3.9	1.3	3.7	34.5
KF007	18Y6M	1.4	-5.7	0.9	30.3
KF008	23Y9M	1.9	-2.4	1.1	27.2
KF009	29Y6M	3.6	-0.9	3.4	31.5
KF010	19Y6M	3.1	-1.3	3.3	34.3
KF011	18Y3M	2.1	-2.4	2.0	35.6
KF013	32Y1M	3.2	0.9	3.9	36.9
KF014	51Y6M	2.1	-0.9	1.7	35.5

2-3. Surface Mapping of the Skull[23]

Following confirmation of skeletal Class I and mesocephalic relationship, the qualifying images were formatted for optimum hard tissue resolution, and the surface of each skull was extracted using a triangular mesh approach that identified a variable number of surface nodes to describe the shape of the skull (Figure 11). Approximately 600,000 triangles and 300,000 vertices were contained in a mesh, but the number of vertices was then standardized to a working resolution and allowed for vertex-vertex correspondence between skulls during alignment. The files were exported in a .PLY format (Polygon File Format).

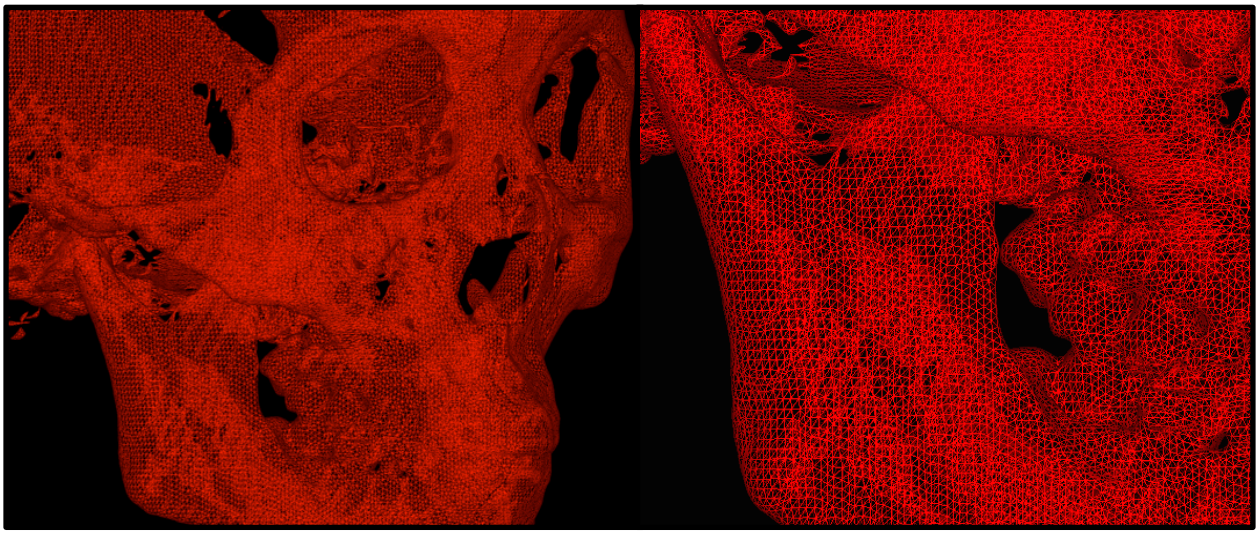

Figure 11: Image of KM001 surface extracted into the intricate triangular mesh surface framework generated in Dolphin Imaging.

Because of the variability of surface topology in the human skull, topology correction must be performed in order to find point-to-point correspondences among samples for averaging and superimposition. Previously, various methods for morphometric surface mapping were proposed, particularly for cortical surface and subcortical structure

mapping in brain imaging.[26,27,28,29] However, developing similar methods for obtaining skull data presents unique challenges due to the following reasons. It is theoretically impossible to determine a well-defined correspondence between surfaces of different topologies, and the low signal-to-noise ratio (SNR) of CBCT images amplifies the surface variability. Therefore, topology correction was accomplished by making each surface topologically equivalent to a sphere (Figure 12).

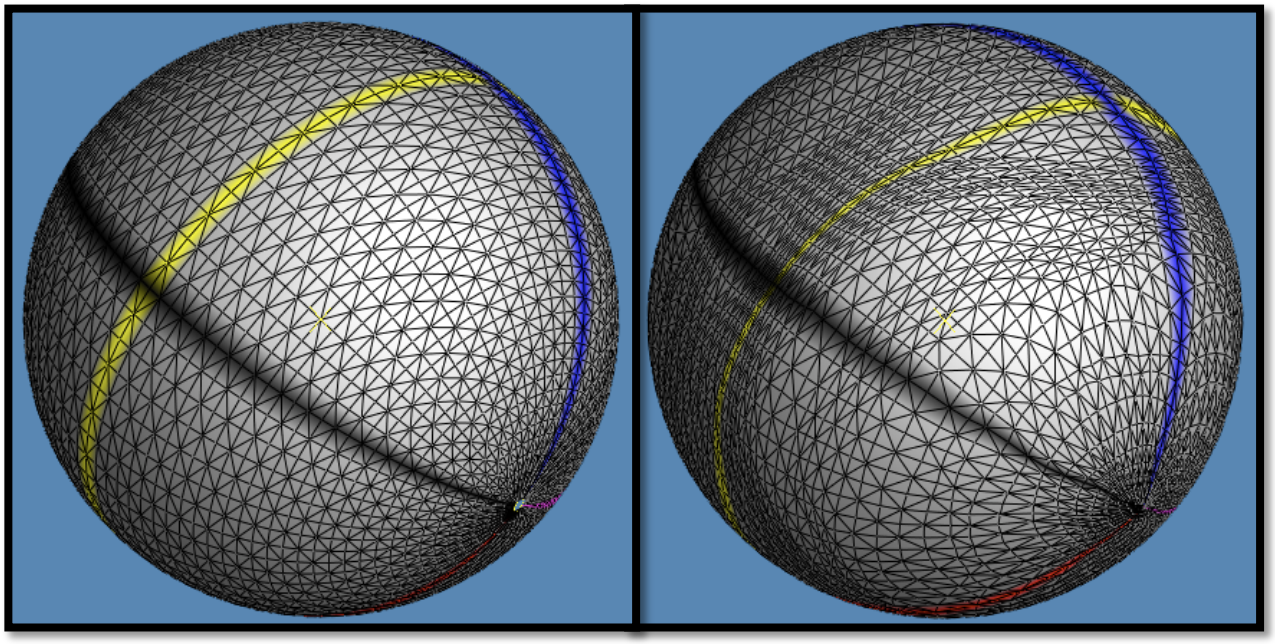

Figure 12: (Image adapted from McComb)[23]. Spherical representation of a skull surface mesh in original and warped form.

Following topology correction, it is critical for the geometry of each shape to remain sufficiently similar to another for the subsequent surface registration to remain robust. The spherical harmonic (SPH) extrapolation approach was used to approximate the shape of the skull, using the principal axis-based star map as the initial partially defined map to approximate SPH coefficients.[30] The method for spherical correction utilized in this study

did not alter the original shape in defined regions while performing more refined smoothing in extrapolated regions.

For the surface registration and establishment of point-to-point correspondence among skulls, we utilized the curve landmarks that were manually picked for defining the boundary information (See 2-4 below). Correspondence between two subjects' skull surface models was established by matching projections of the curve landmarks to the spherical domain. As each skull has its own unique spherical map naturally arising from the harmonic interpolation procedure, the projection was a straightforward additional step (Figure 13).

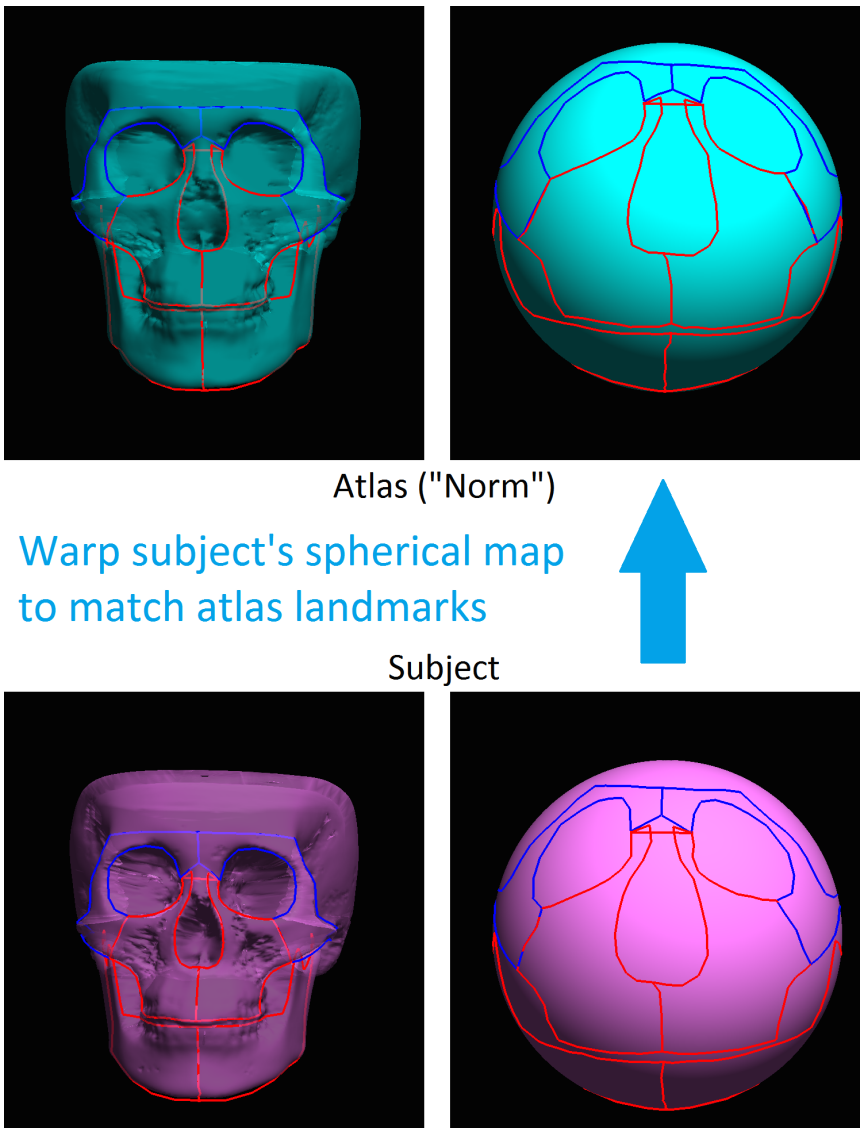

Figure 13: Spherical map projection of the surface and curve information. To establish correspondence, subject's spherical map is warped to match atlas "norm" landmarks.

Next, elastic landmark matching via a smooth invertible warp of a moving subject's map was imposed to make corresponding points of the target subject as close on the sphere as possible. Following the warp, the moving surface model can be resampled spherically for exact pointwise correspondence. A similar procedure constructs a sample norm, or "atlas," as detailed below. This was an improved approach from the previously utilized spherical patch mapping method, which required a few manually marked landmarks on a

template skull that were then automatically identified on other samples for establishing correspondence.[31]

2-4. Extraction of the Skull Outline Information[24,25]

The outline information of the craniofacial structure was based on an interface developed for a previous study by Drs. Khullar, Soares, and Sung. Following hard tissue optimization, the 3D image was sectioned into seven different specific regions of interest for the purpose of defining the outline of the mandible, maxilla, and cranial base. Along each of the anatomic borders of the mandible, maxilla, and cranial base, a total of 104 points, 92 points, and 117 points were be picked respectively (Figure 14).

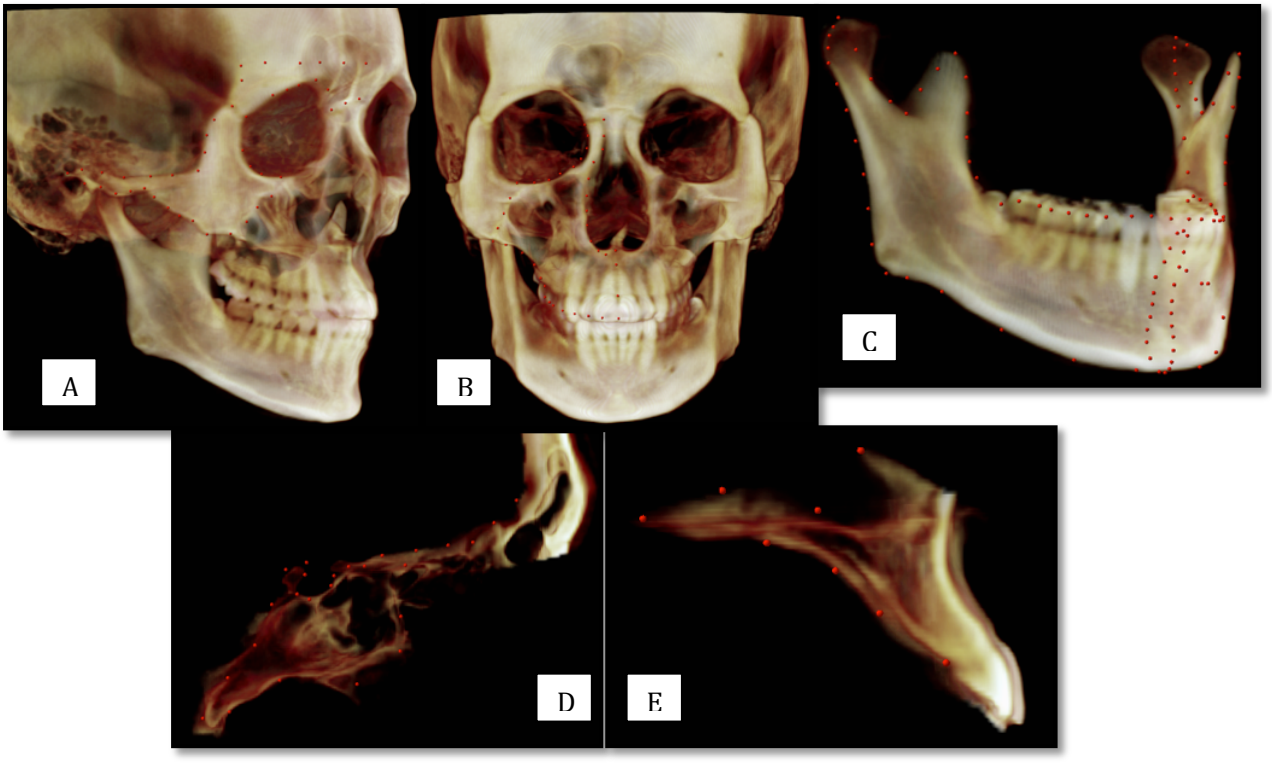

Figure 14: Snapshot of collecting points for subject KM001. (A) Right Zygoma, (B) Right Maxilla, (C) Mandible, (D) Mid Cranial Base, (E) Palate.

The measurements utilizing point coordinates (x, y, z) were made in millimeters and recorded into a text file format (.txt), which was subsequently used for geometric alignment and analysis.[24] Correspondence of points in each component was assumed based on manual digitization. Assuming existing correspondence, we sought an average position, size, and orientation – the mean affine transformation – of the average shape.

2-5. Normalization

The 'average pipeline' was created to process both the surface (.PLY file) and boundary (.txt file) information of the subjects to create the average (Figure 15). The shape models were first aligned in their original (non-parametric) space based on the computed dense correspondence, and a single subject was chosen to serve as the target for all alignments. Then, the 7-parameter Procrustes method[31] was used, allowing normalization of the skull shape and curve outline under the best-fit registration and size standardization. Once the normalized form of the curve and surface was obtained, each part was aligned in the correct position in relationship to the other, utilizing common points as references to merge the two different types of information.[23,25]

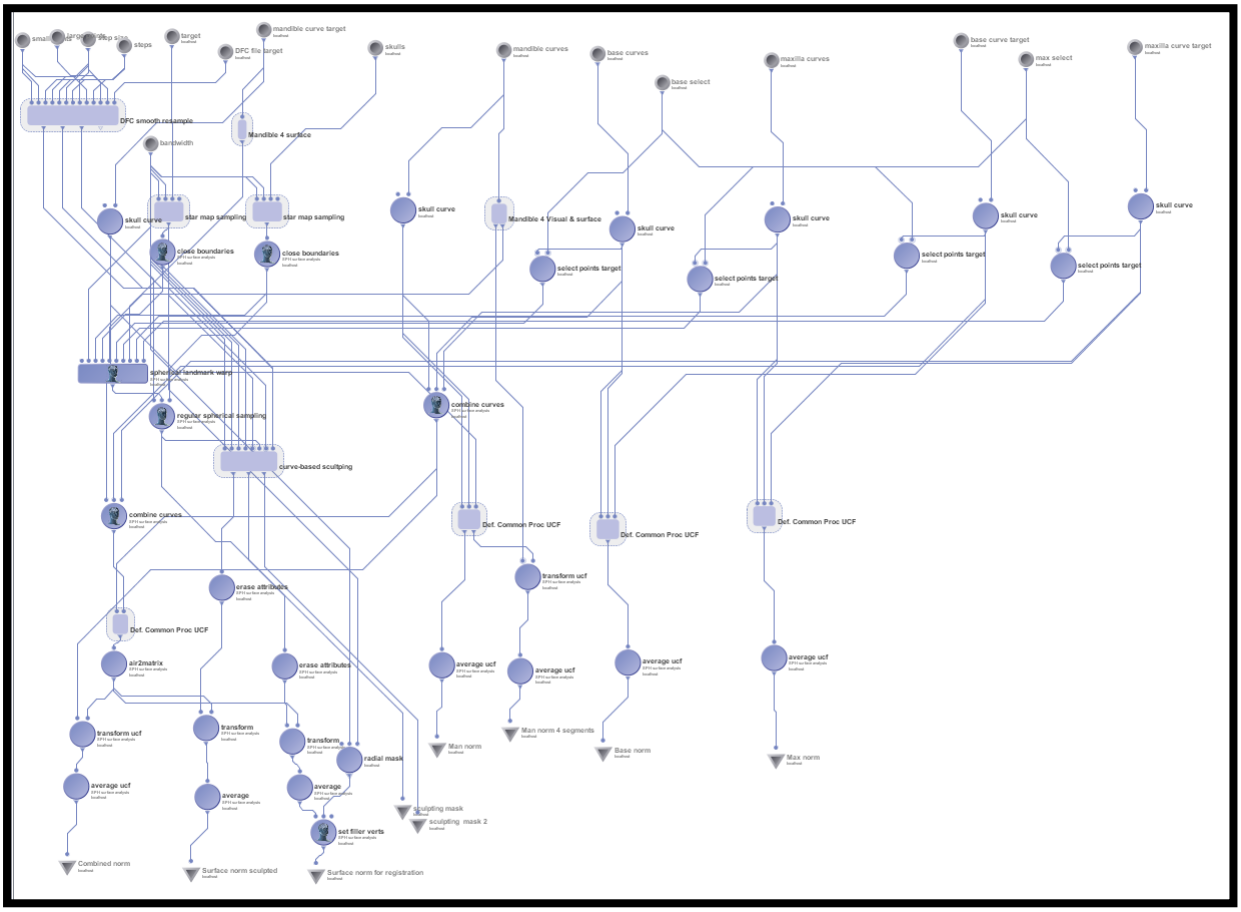

Figure 15: Snapshot of the 'average pipeline.' The surface and boundary information was input into the pipeline and run through various steps to create the average.

2-6. Superimposition – Distance, Vector, and Statistical Maps

After computing the average skull shape, the distance from the average to each individual shape and the standard deviation at each point can be found. Distance-to-average maps are displayed as colorized surface maps, a key feature that will allow for comparison of a patient's CBCT image to the respective sub-norm. For this study, one subject from the original male and female group was selected as the internal sample for comparison. An external subject with apparent skeletal disharmony was selected as well to represent a case that greatly deviated from the normal sample. Both the internal and external

subjects were then compared to the sub-norm in order to display the clinical effectiveness of the colorized map. In addition to the distance-to-average color map, a vector map was created to show the direction and magnitude of the compared subject's displacement from the sub-norm in three planes of space. Since the distance map simply illustrates the absolute value of the displacement of each vertex to the norm, the vector map is clinically useful in identifying the directional information of severely deviated areas. As mentioned above, each vertex (x, y, z) carries its own statistical value of its degree of displacement in standard deviations from the normative model. Thus, a colorized statistical map was generated to illustrate the standard deviation of the distance to the mean at each vertex along the surface.

3. Results

3-1. 3D Korean Adult Male and Female Skull Average

A comprehensive review of CBCT scans that qualified the inclusion and exclusion criteria resulted in 11 Korean male and 13 Korean female samples. The sample population displayed a class I skeletal relationship with minimal topological variability. The scans were entered into the developed pipelines and subjected to the methods proposed above, including topology correction and shape registration. The 'average' pipeline required about 10 minutes per group to process the samples and create an average. The respective output result showed a smooth and harmonious skull model seen in the various views below (Figures 16-17).

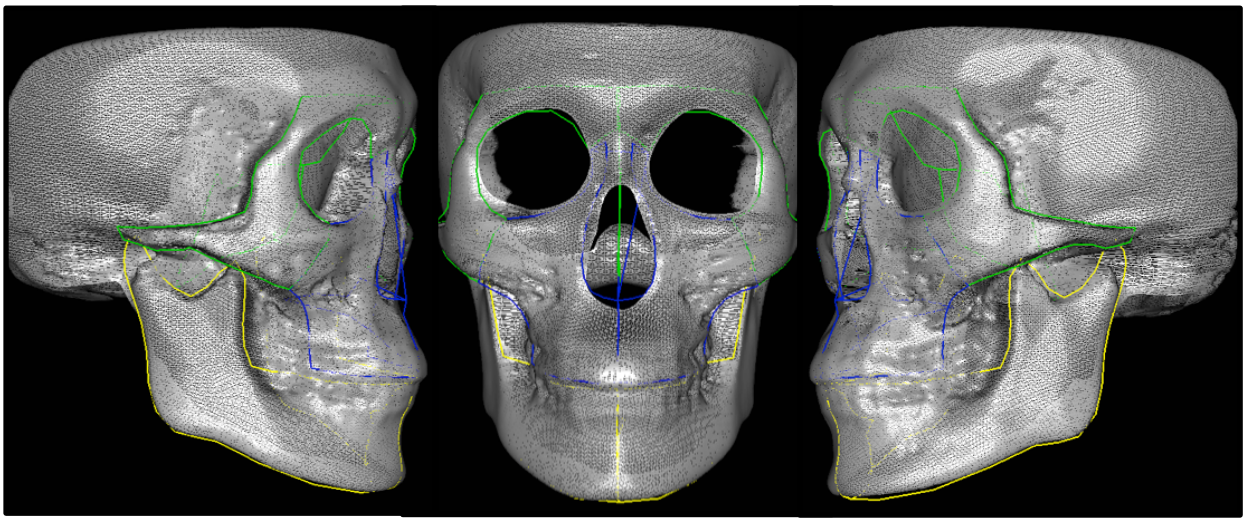

Figure 16: 11 sample average - Korean male subnorm – shown in right lateral, frontal, and left lateral views.

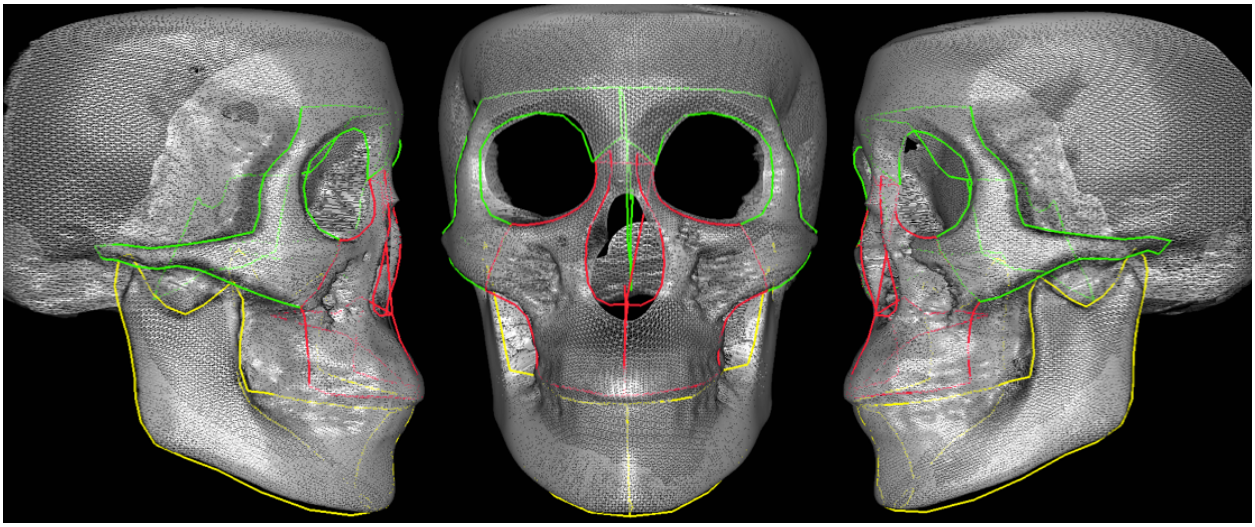

Figure 17: 13 sample average - Korean female norm – shown in right lateral, frontal, and left lateral views.

3-2. 3D Superimposition of Individual Sample to Average

After development of an average skull normative model from the 11 male and 13 female image sample, our registration technique was applied to demonstrate the ability to

superimpose a sample individual 3D skull image on the average model utilizing the newly developed 'superimposition' pipeline (Figure 18). The orientation of the mesh framework was maintained, allowing point-to-point correspondence of vertices to be retained within the average skull.

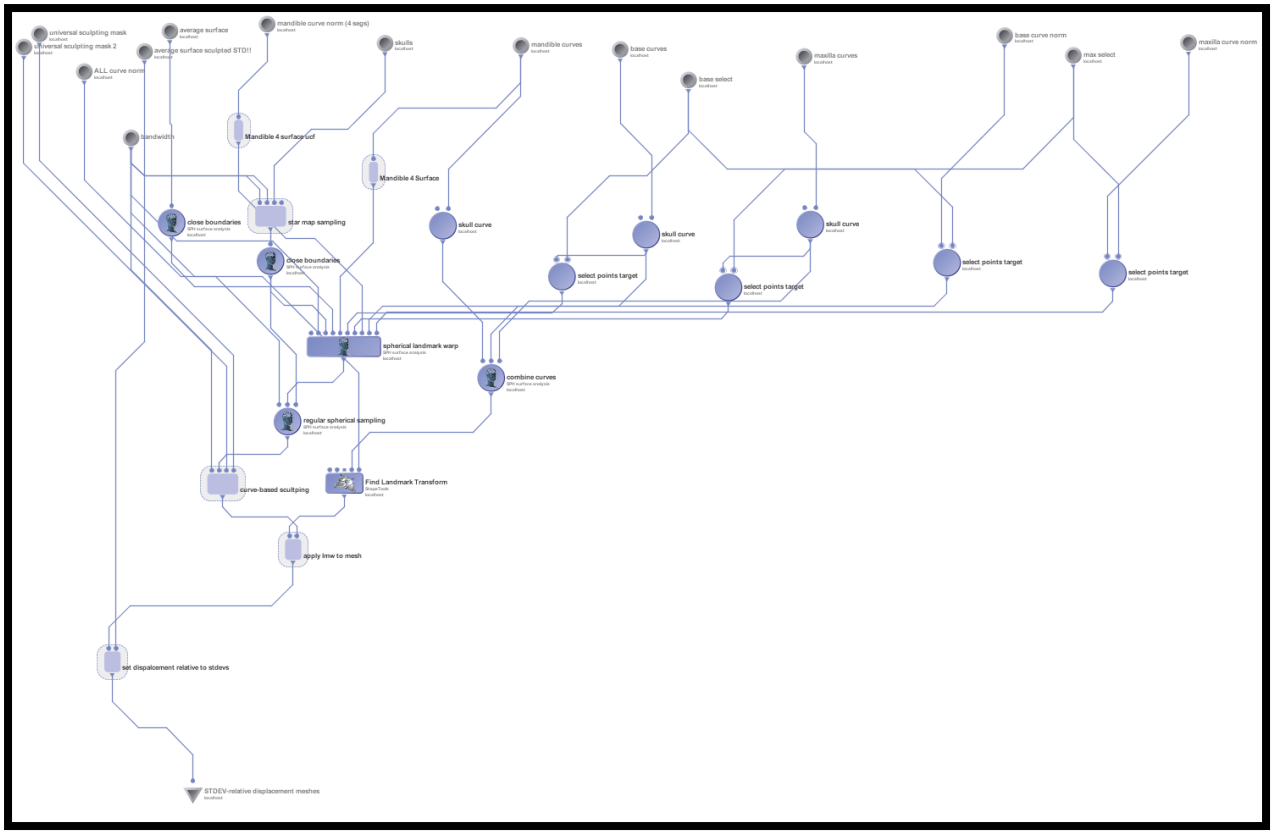

Figure 18: Snapshot of the 'superimposition' pipeline used to calculate the linear displacement values and standard deviations.

3-2.1. Linear Distance Map

The next step in producing clinically applicable superimpositions is to develop color-coded maps of surface deviation and dysmorphology. Colorized displacement maps offer the ability to set threshold values for each color. The spectral color scheme that we chose

to represent the absolute value of linear displacement values were as follows: Purple represents minimal deviation and Red represents maximal deviation from the norm. The users have the ability to set the minimal and maximal deviation values to see the surface dysmorphology. The magnitude of displacement in this study was set from 0mm to 10mm (Figure 19 – 20). In the image seen in Figure 18B, the male sample skull – KM001 – does not display notable linear displacement compared to the norm except in the anterior nasal spine and A point region. This area can be further analyzed in the vector and statistical maps for a possible explanation of such increased deviation. On the other hand, the female sample skull, KF001, superimposition did not illustrate any significant deviations from the norm, as expected (Figure 20).

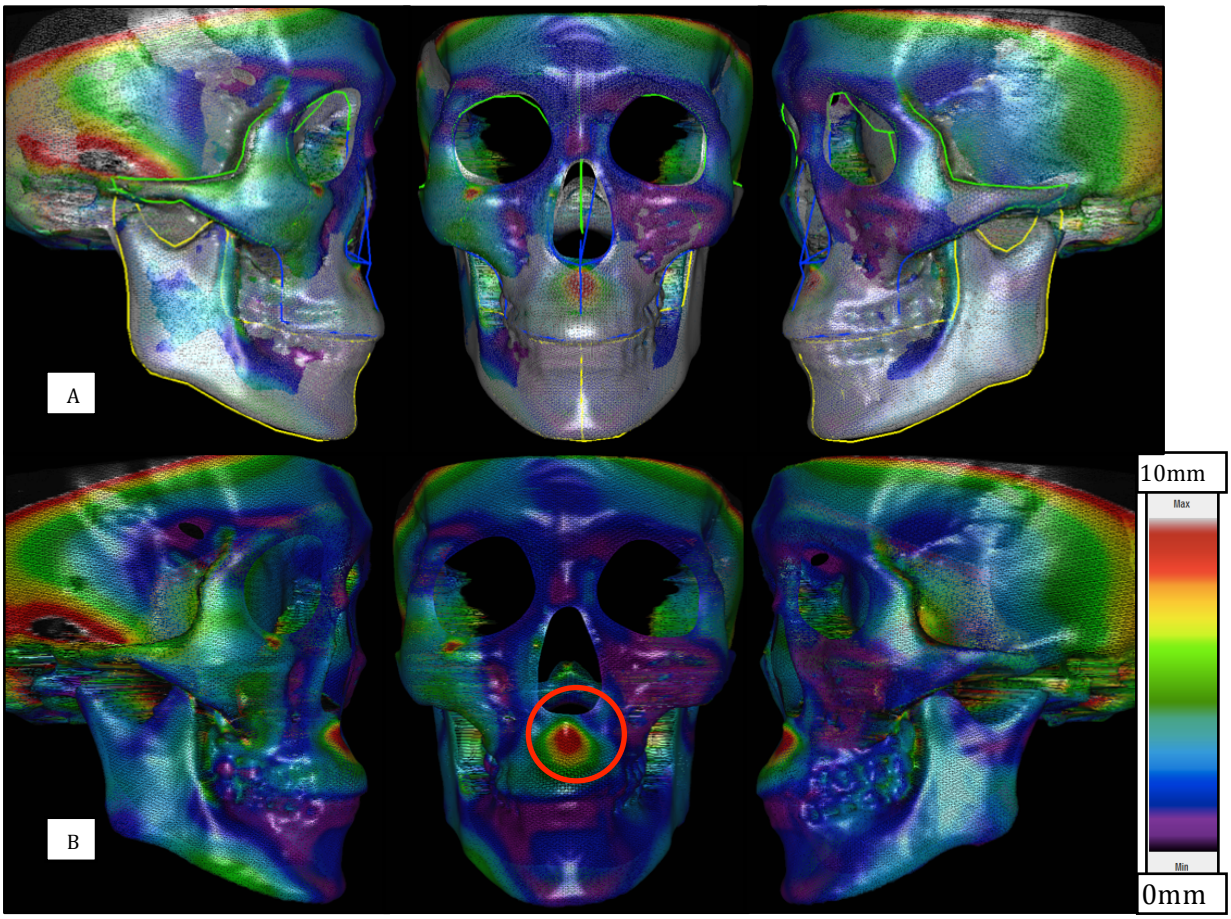

Figure 19: (A) A linear distance color map of a male sample, KM001, superimposed over the male average subnorm. (B) KM001 represented in multiple colors without the average. Min value is 0 mm and max value is 10 mm.

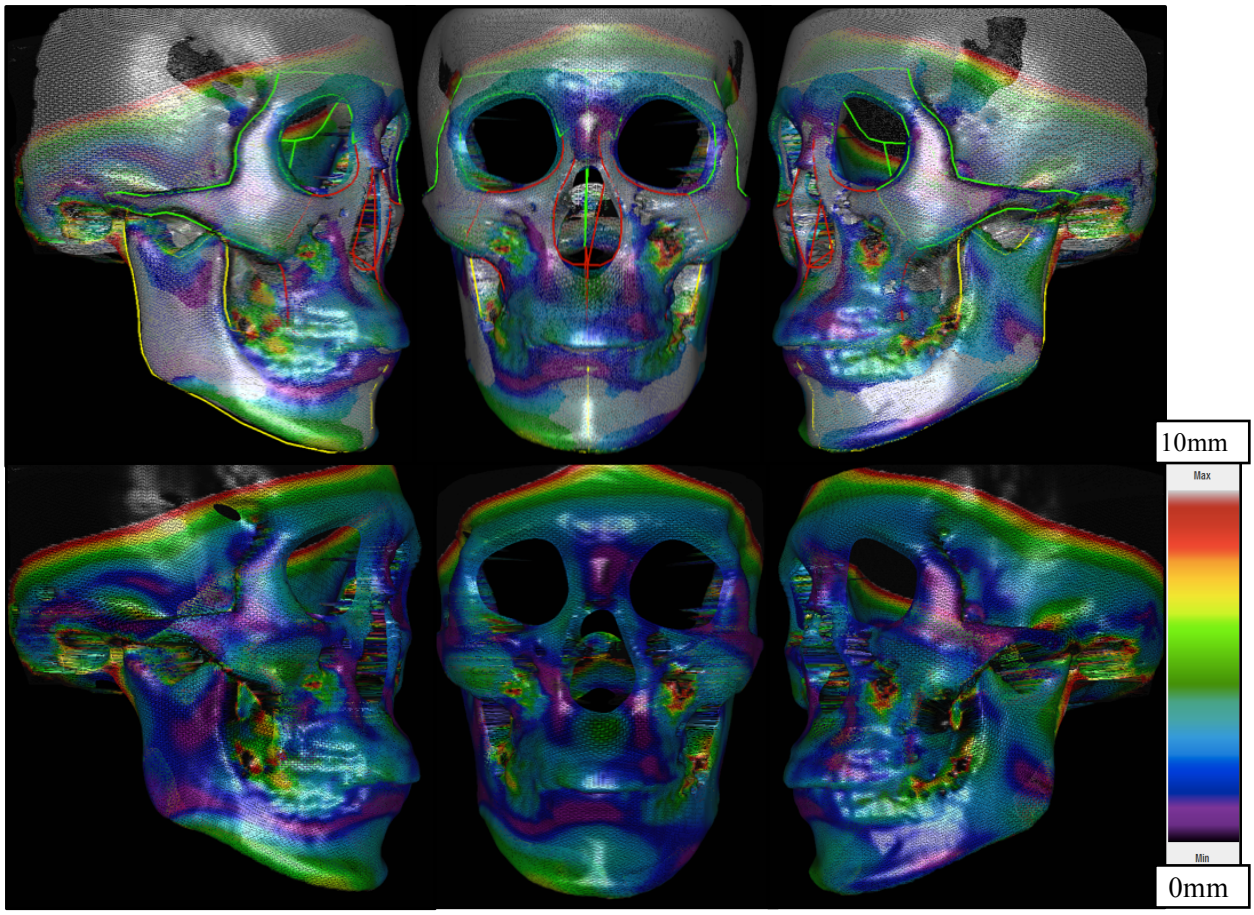

Figure 20: (A) A linear distance color map of a female sample, KF001, superimposed over the female average subnorm. (B) KF001 represented in multiple colors without the average. Min value is 0 mm and max value is 10 mm.

3-2.2. Vector Map

The establishment of vector maps is a critical addition to 3D analysis because it provides important supplemental information to the linear distance maps (Figure 21). Vector maps allow users to see the direction and magnitude of surface dysmorphology that can intially

be observed with the colorized distance maps. Although we can have a vector arrow for all 250,000 vertices along the surface, this is not optimal for viewing. Thus, the number of arrows was reduced and optimized for viewing. Brainsuite15b software was used for viewing, and its function that allows users to zoom in and out of relevant areas of the skull was beneficial in closely evaluating variation at a given point or region (Figure 23). Based on the vector map superimposition, the 'red' region as noted in Figure 19B appeared to be due to KM001's ANS and A point region positioned superior and posterior relative to the norm. Thus, the vertical height difference of KM001 and the norm's maxillas would be the logical explanation instead of the anterior-posterior discrepancy. Figures 22 and 24 show the vector maps of the same KM001 and KF001 scans superimposed over respective subnorms.

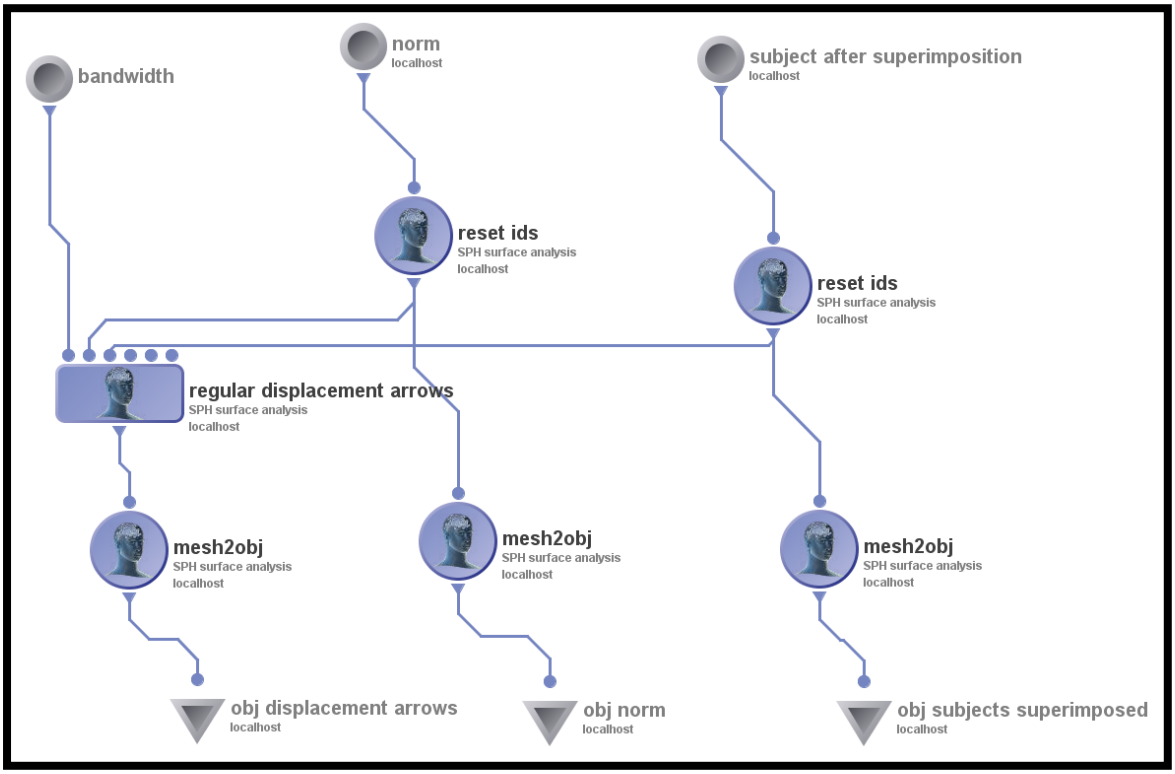

Figure 21: *Snapshot of the 'vector map' pipeline.*

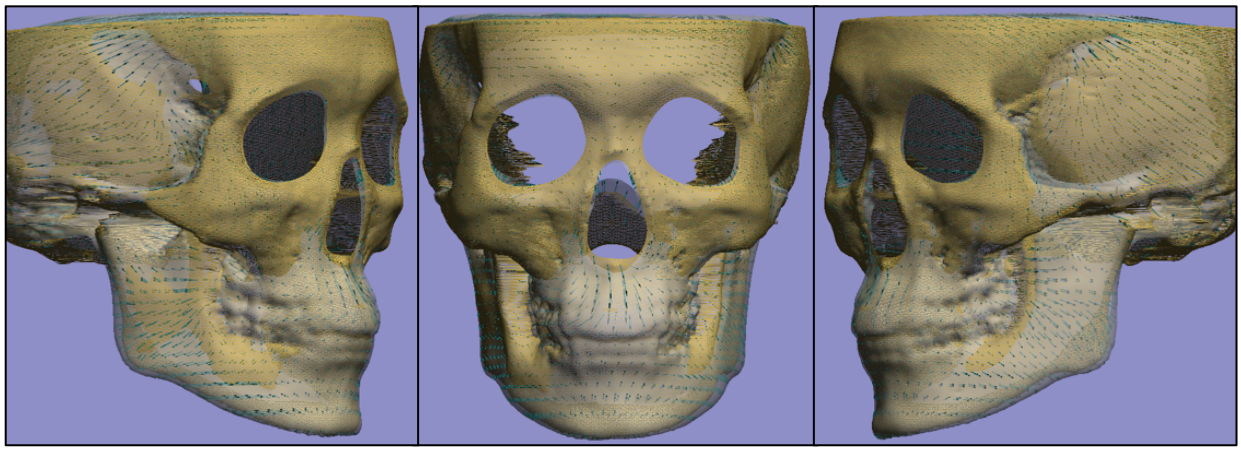

Figure 22: Vector map of a male sample, KM001, superimposed over the male subnorm in right lateral, frontal, and left lateral views. The norm is translucent and KM001 is displayed in wireframe.

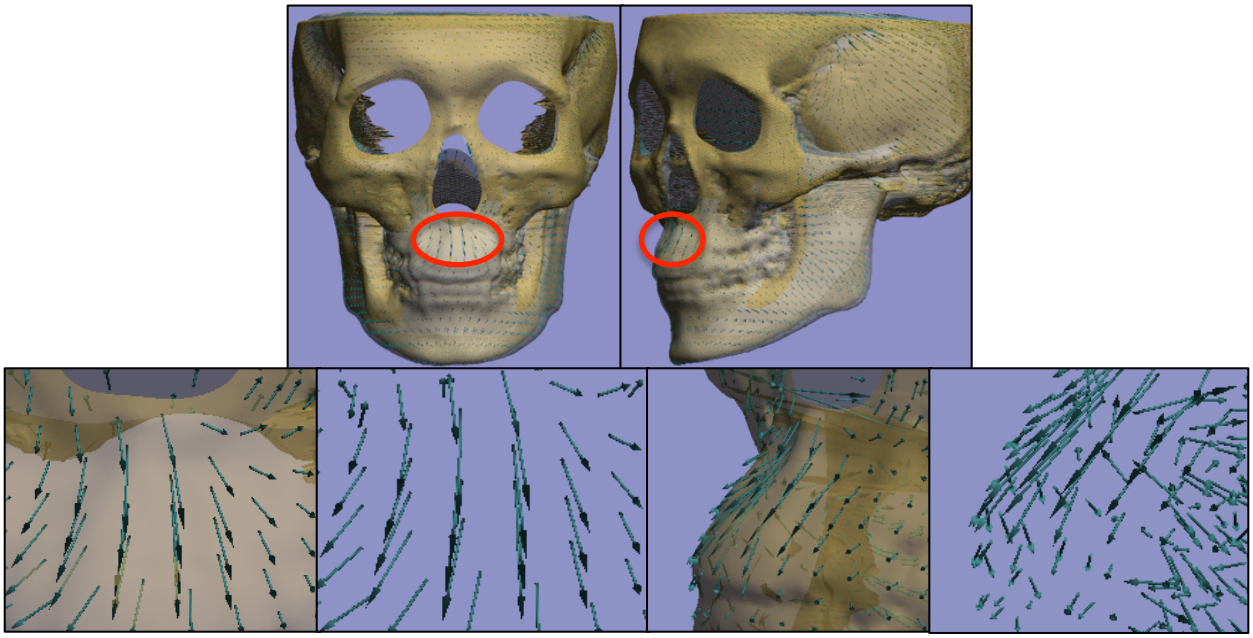

Figure 23: The 'red' colorized area from the linear distance map in Fig 18B is zoomed in to visualize the displacement direction.

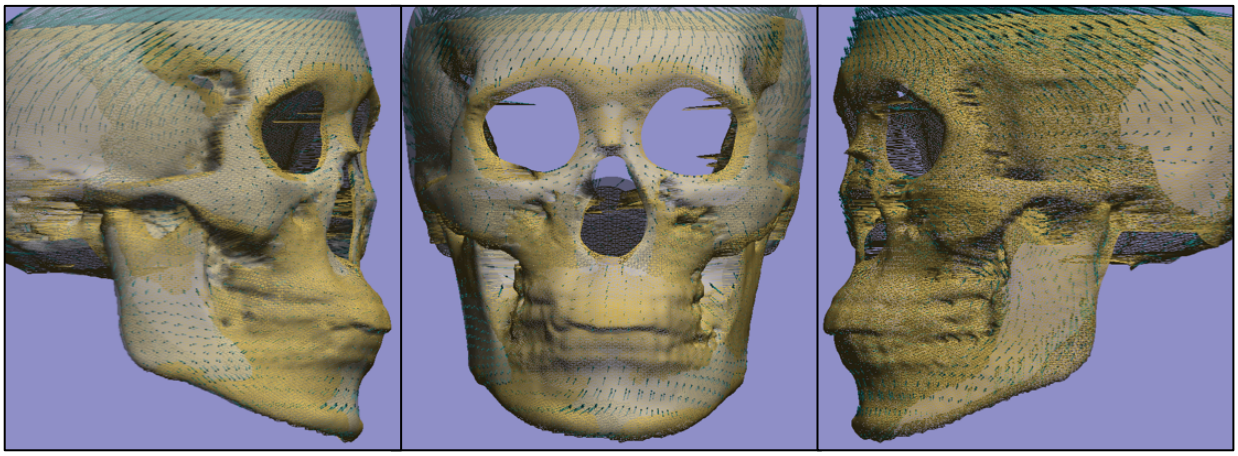

Figure 24: Vector map of a female sample, KF001, superimposed over the average in right lateral and frontal views. The left lateral view shows the image without the female subnorm. The norm is translucent and KF001 is displayed in wireframe.

3-2.3. Statistical Maps

Statistical maps based on distance to the average were created, involving parametric or non-parametric (e.g. permutation) statistical tests done at each point, which localize the effect of the biological variable on the skull surface.[26] The statistical pipeline generates the standard deviation of the Euclidean distance to the mean for each vertex and we are able to illustrate it through colorized statistical maps. Although the minimum and maximum standard deviations are calculated through the software, users have the ability to set these values. Figure 25 illustrates the colorized statistical map of KM001, and the minimum and maximum were rounded to the nearest number. For even more user-friendly viewing, we simplified the spectral color scheme to three colors – blue, green, and red – with areas within 1, 2, and greater than 2 standard deviations respectively (Figure 26). Figures 27 and 28 show the same example for KF001.

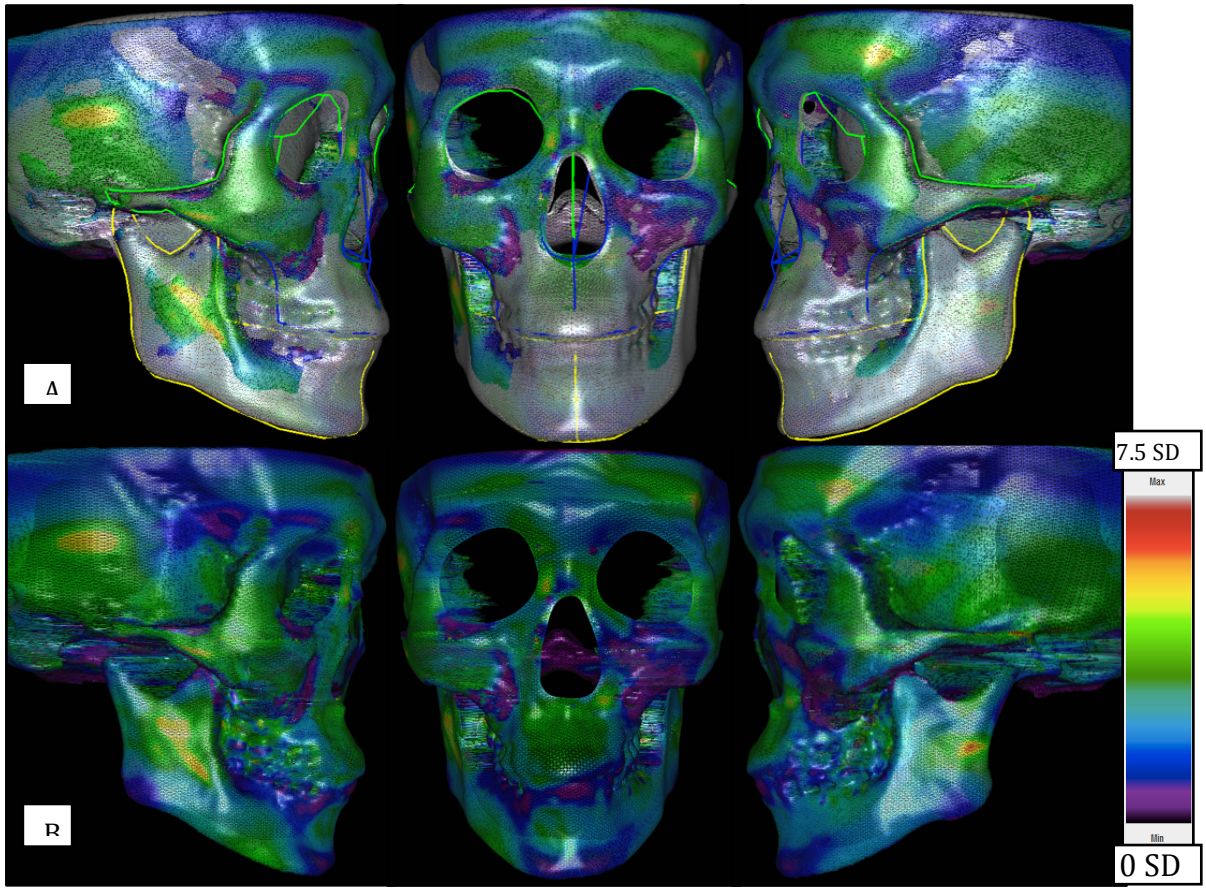

Figure 25: (A) Statistical map of a male sample, KM001, superimposed over the male subnorm. (B) KM001 shown without the subnorm. The absolute value of the standard deviation (SD) of the Euclidean distance to the mean is compared to the norm. Min value is 0 SD and max value is 7.5 SD.

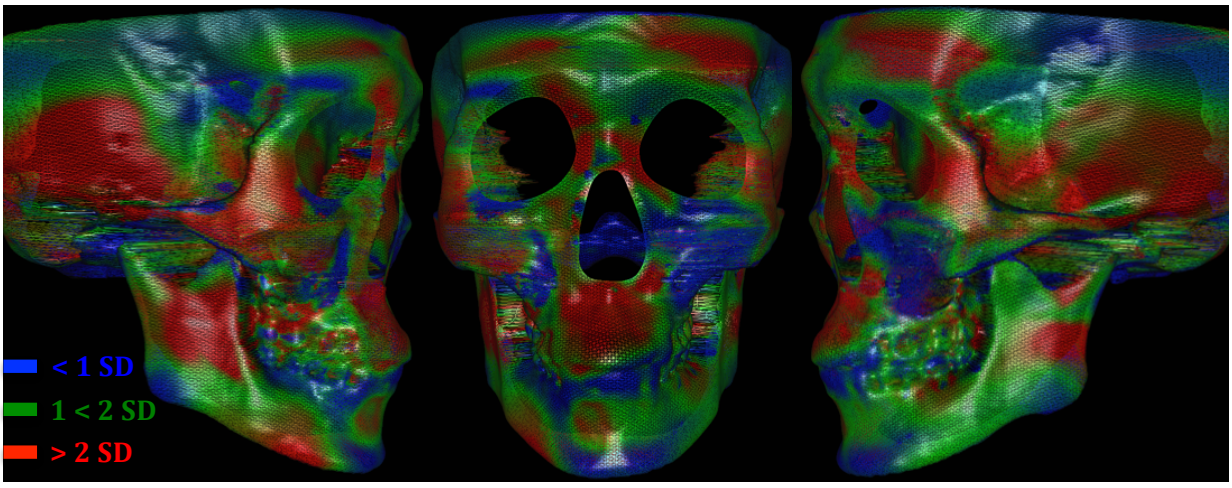

Figure 26: Simplified statistical map of KM001 represented in three colors – blue, green, red – with respect to standard deviations.

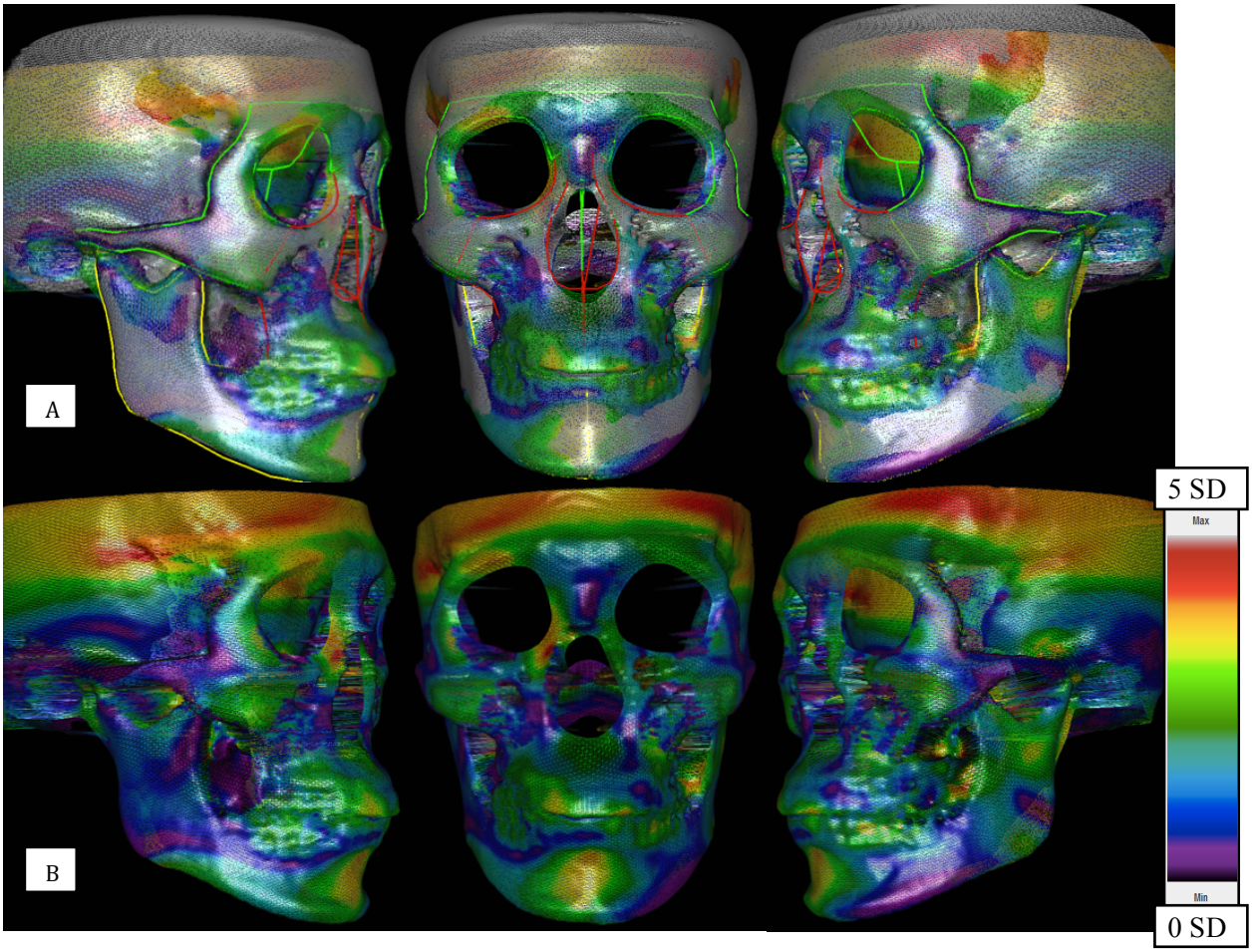

Figure 27: (A) Statistical map of a female sample, KF001, superimposed over the female subnorm. (B) KF001 shown without the subnorm. The absolute value of the standard deviation (SD) of the Euclidean distance to the mean is compared to the norm. Min value is 0 SD and max value is 5 SD.

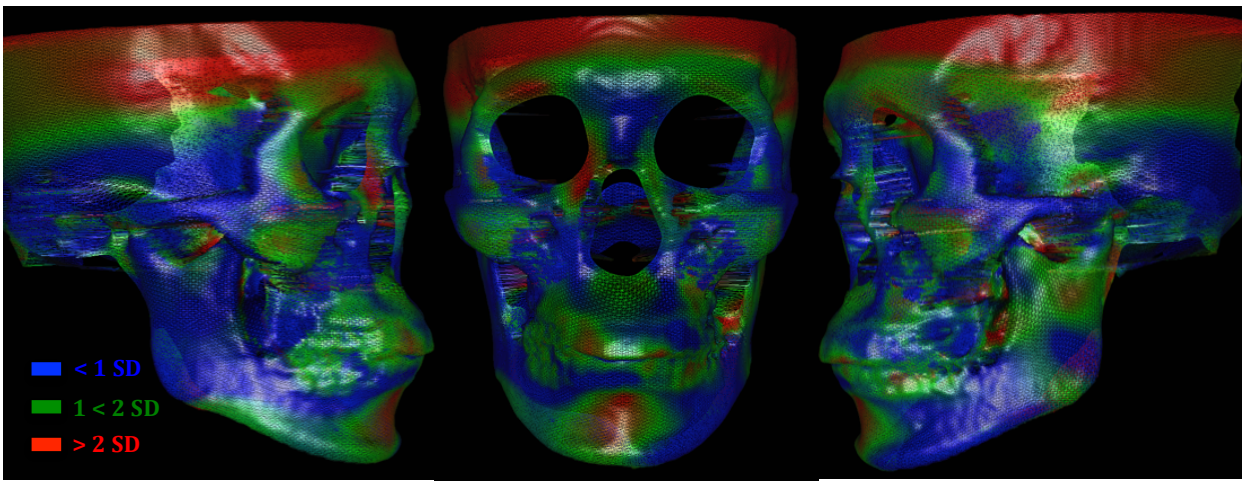

Figure 28: Simplified statistical map of KM001 represented in three colors – blue, green, red – with respect to standard deviations

It is particularly useful when looking at all three maps together for analysis as shown in Figure 29. You can locate the areas of increased deviation in 'Red' and easily visualize the direction and statistical significance.

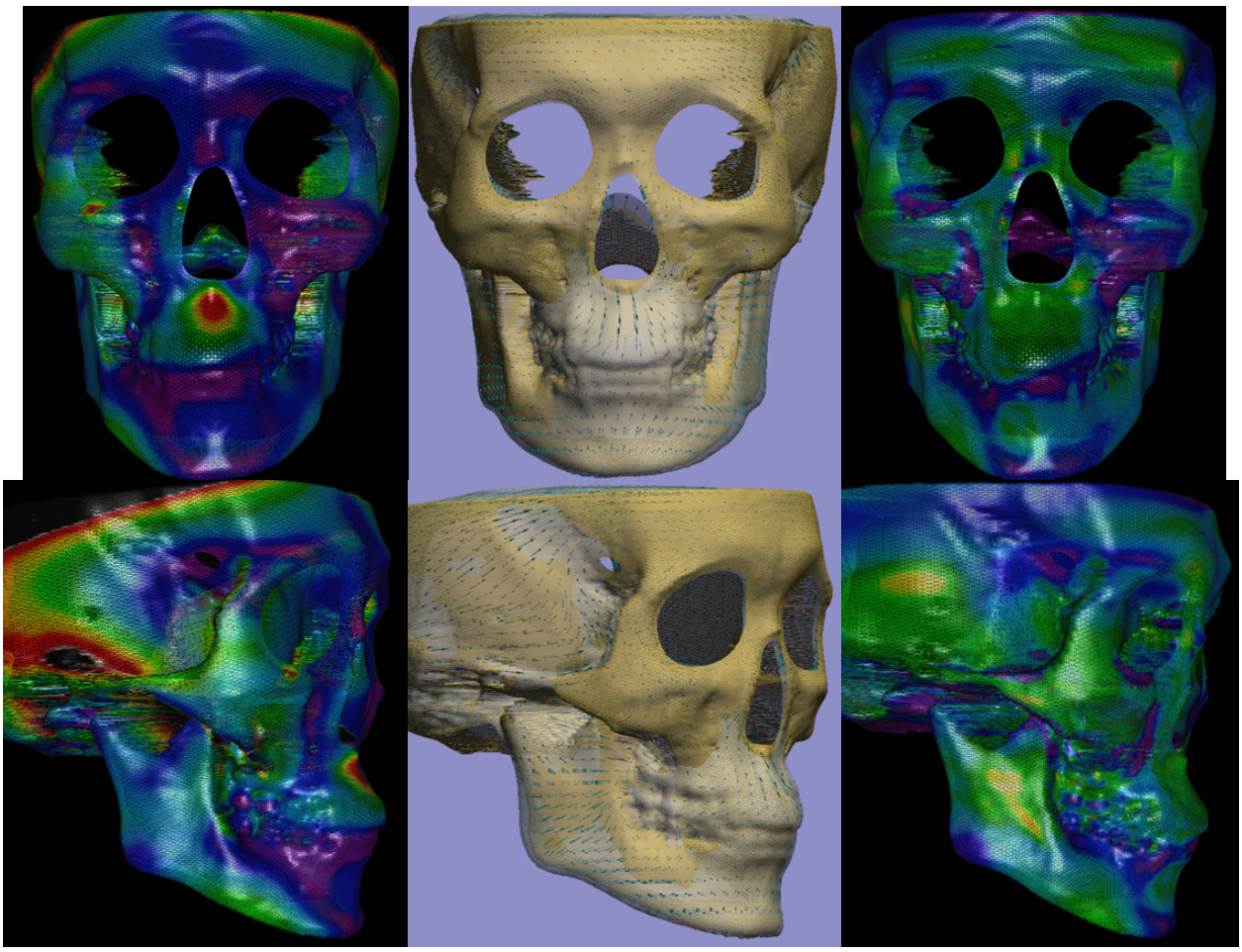

Figure 29: Linear displacement, vector map, and statistical maps of KM001 viewed side by side in frontal and right lateral views.

3-3. 3D Superimposition of an External Subject with the Norm

A 20-year-old Korean male patient with a diagnosis of Class III skeletal pattern (ANB = -6.7, Wits = -13.9, Convexity = -8.5) was selected as the external, abnormal sample to be superimposed and compared with the male subnorm. Looking at the CBCT scans in various views, one can generally diagnose that this patient presents a retrognathic maxilla and a prognathic mandible (Figure 30). However, we can appreciate that the maxilla is

more greatly affected than the mandible in three planes of space, as illustrated in the linear distance, vector, and statistical maps (Figures 31 – 35).

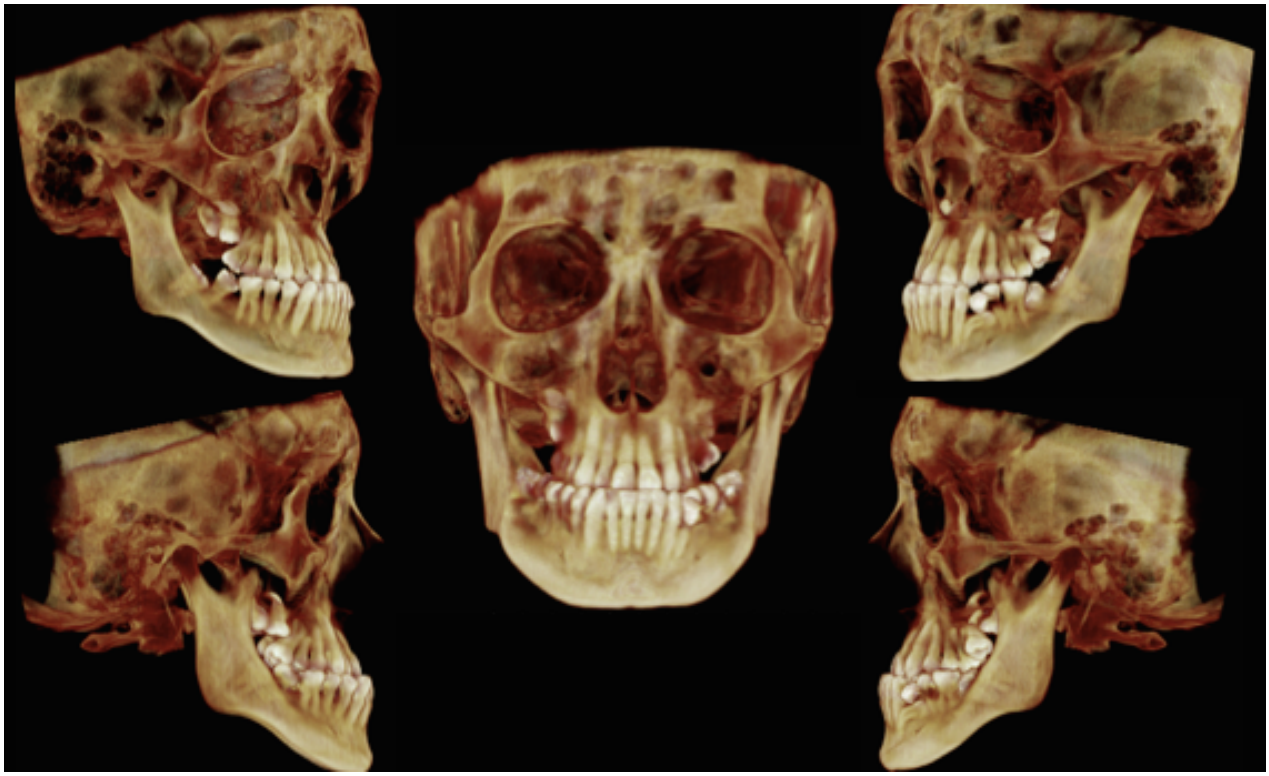

Figure 30: CBCT image of skeletal Class III patient, KM017, used as the external/abnormal sample for comparison to the male subnorm.

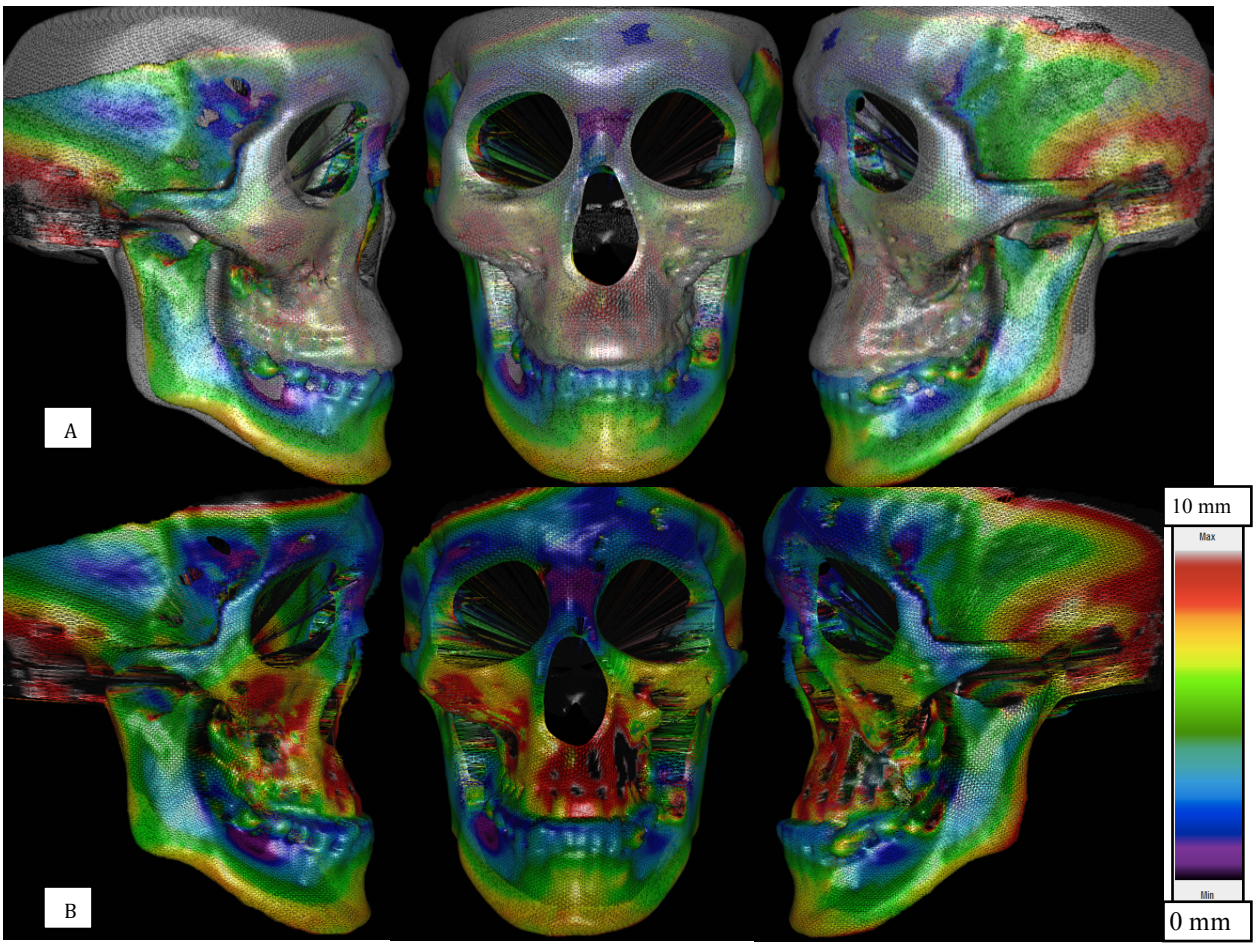

Figure 31: (A) A linear distance color map of the external/abnormal sample, KM017, superimposed over the male average subnorm. (B) KM001 represented in multiple colors without the average. Min value is 0 mm and max value is 10 mm.

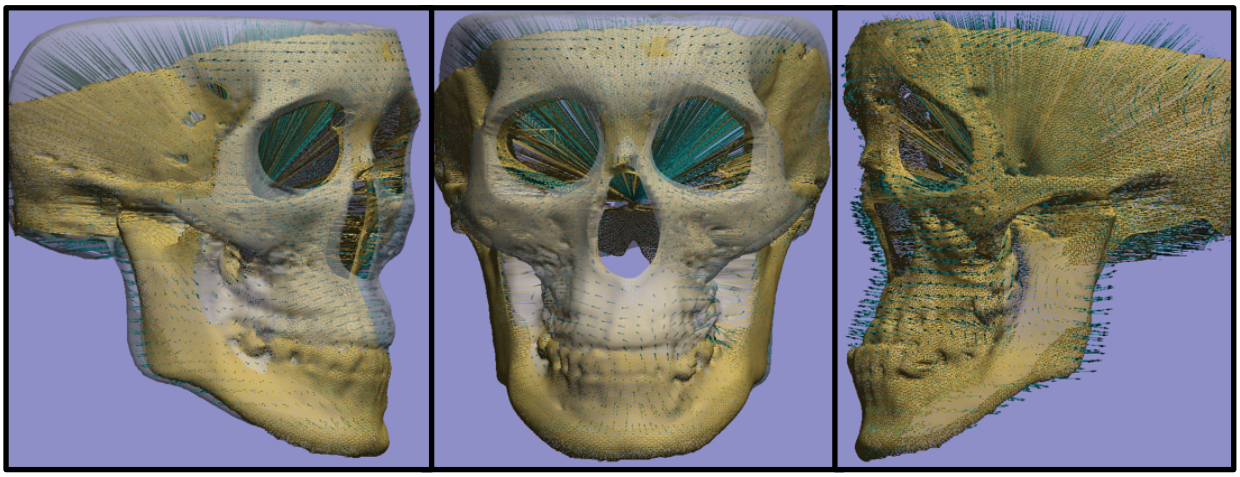

Figure 32: Vector map of the external/abnormal sample, KM017, superimposed over the male subnorm in right lateral and frontal views. The left lateral view shows the image without the average. The norm is translucent and KM017 is displayed in wireframe.

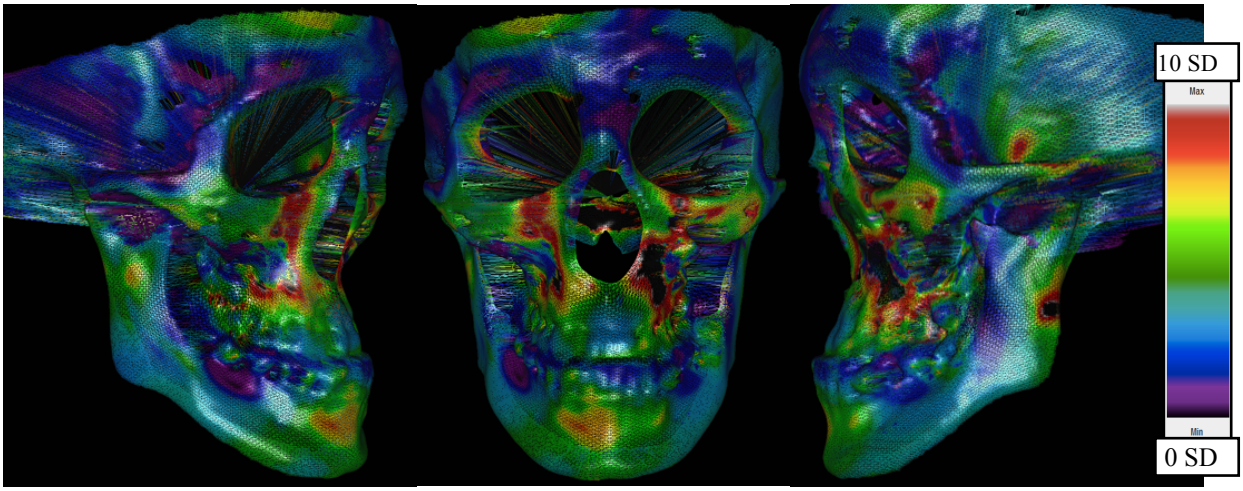

Figure 33: (A) Statistical map of the external/abnormal sample, KM017 without the subnorm. The absolute value of the standard deviation (SD) of the Euclidean distance to the mean is compared to the norm. Min value is 0 SD and max value is 10 SD.

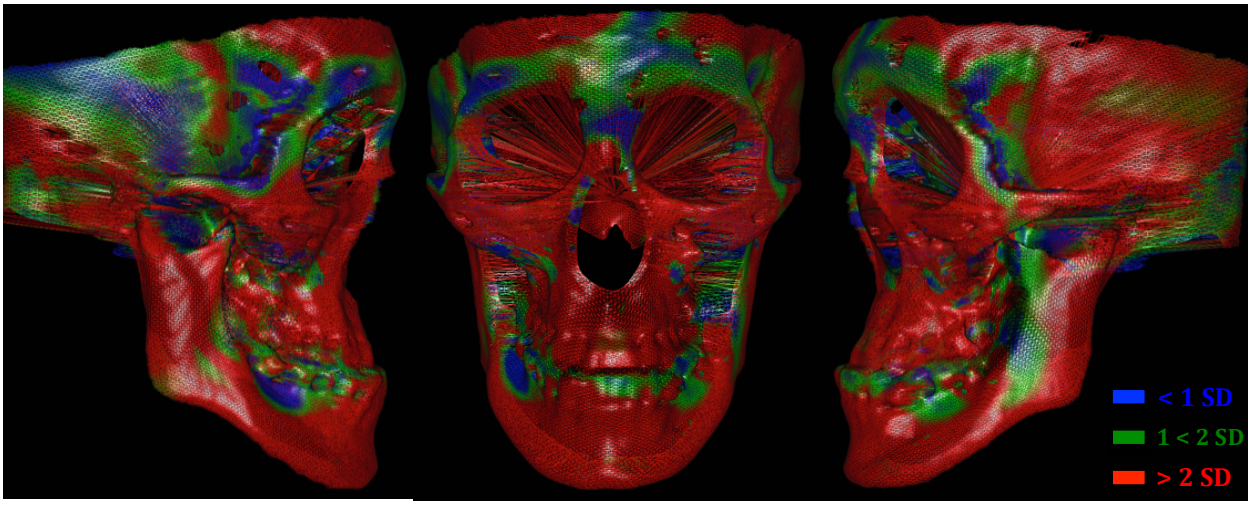

Figure 34: Simplified statistical map of KM017 represented in three colors – blue, green, red – with respect to standard deviations.

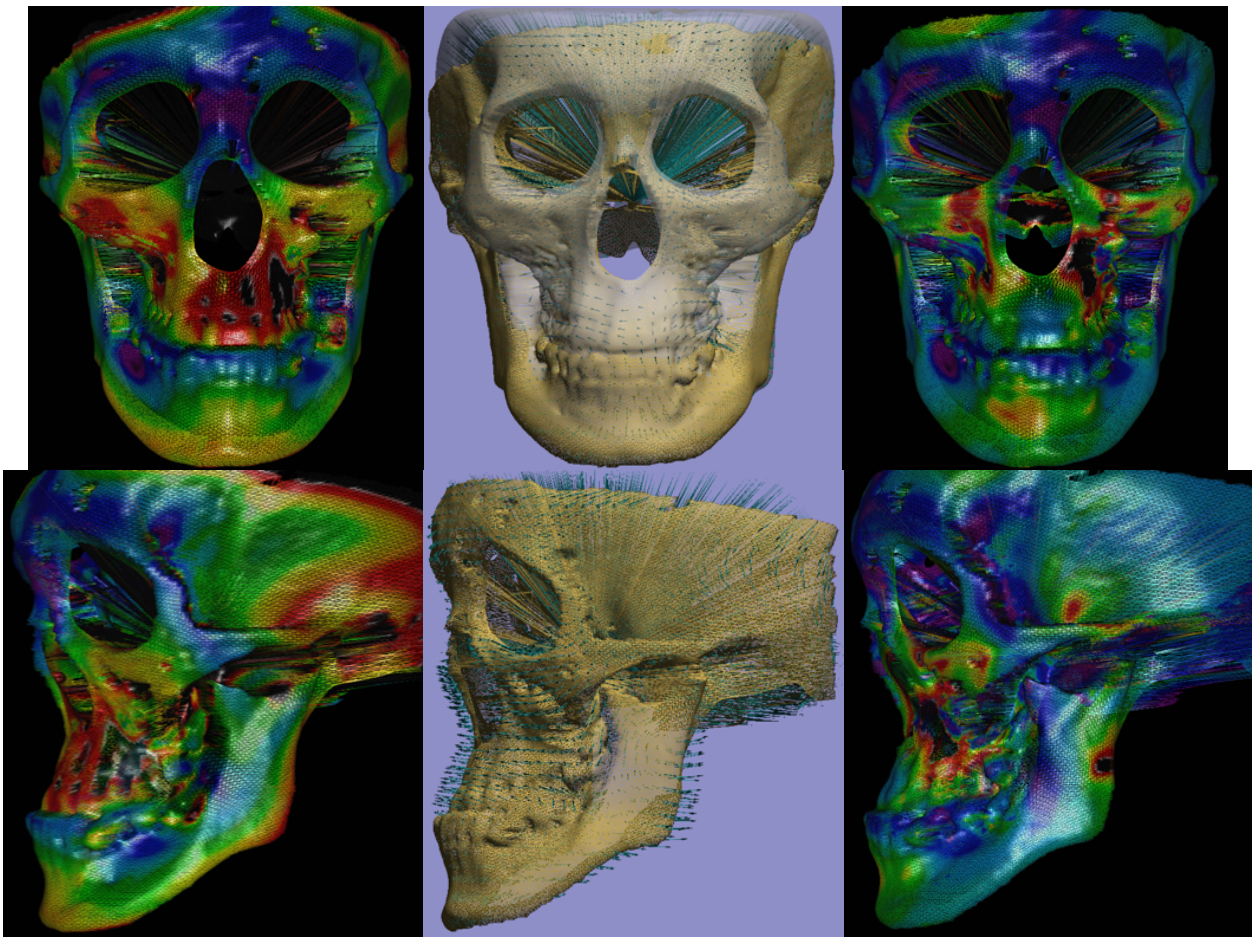

Figure 35: Linear displacement, vector map, and statistical maps of KM017 viewed side by side in frontal and left lateral views.

3-4. Male vs. Female Comparison

Since Korean male and female sub-normative skulls were established, we can size-standardize and compare the two averages. Two sub-norms were superimposed over each other and the mean differences were mapped and illustrated by vector arrows as shown in Figure 36.

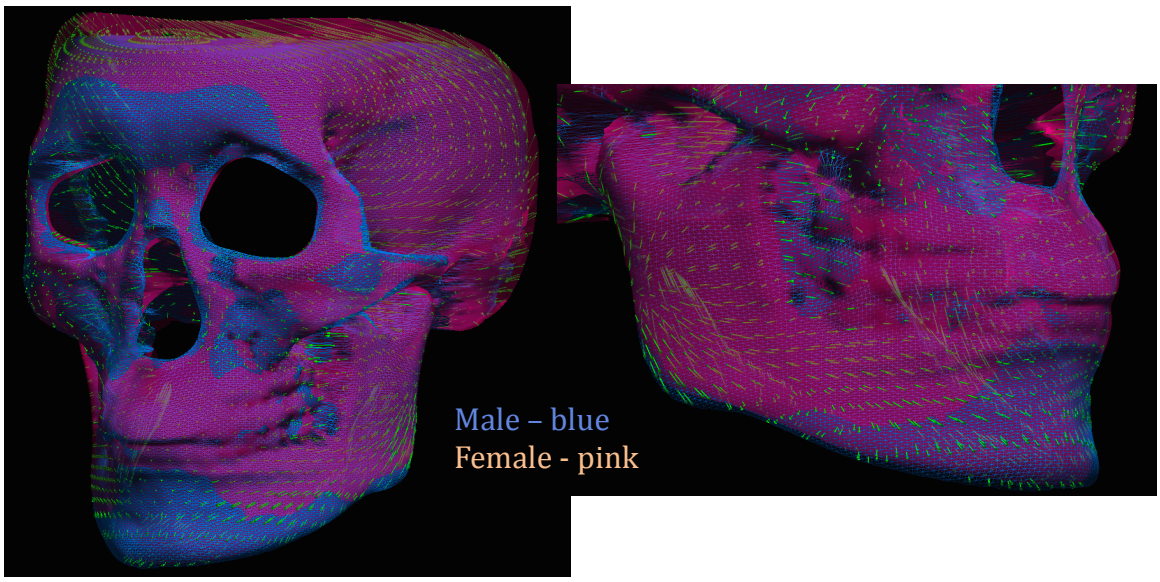

Figure 36: Korean male sub-norm vs. female sub-norm superimposed over each other and the mean differences were displayed with vector arrows.

In addition, we can map the statistical significance of those differences as total displacement or with respect to x, y, z directions (Figure 37). As illustrated in the figure, the mean differences with respect to total displacement between Korean male and female sub-norms were generally not significant except in some areas such as the condylar neck and posterior alveolus. With respect to x, y, z directions, male and female showed significant differences in the mandible.

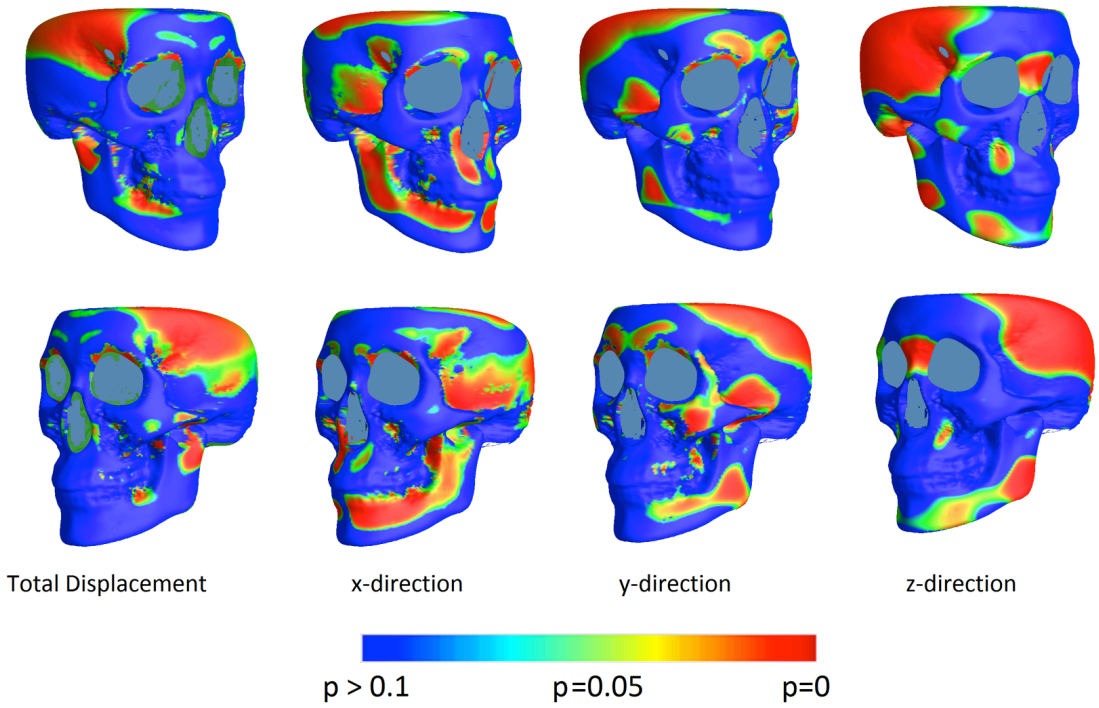

Figure 37: P-map mapping the significance of the Korean male vs. female sub-norm differences.

4. Discussion

4.1 Clinical Application

This study successfully applied the previously developed methods of averaging 3D skulls to create sub-normalized skull models of Korean male and female adult samples. The study demonstrated clinical utility by developing colorized displacement maps, vector maps, and statistical maps of a sample shape compared to the respective average.

The Materials and Methods section of this thesis details the steps necessary to achieve the specific aims of the project. Several pipelines were developed with collaboration from

Dr. Boris Gutman from LONI, and an intricate series of steps within the pipelines allows users to input any combination of patient skulls for averaging, calculating displacement, deriving statistics, and creating vector maps. As shown above, a single skull can be superimposed on the sub-norm utilizing the Procrustes alignment in order to evaluate morphological variation.

In orthodontics, one of the primary goals is to arrive at a proper diagnosis of the case and thus an appropriate treatment plan. For over a decade, clinicians have depended upon 2D cephalometric films and the normative data that accompany them to better understand a patient's skeletal and dental relationship. Recent years have seen a steady increase in the use of CBCT images, particularly in complex cases involving severe skeletal and dental anomalies. In spite of the rise in the popularity of 3D technology, little focus has been placed on the need to establish new analyses that take full advantage of the additional information provided by CBCT images. Instead, most studies have applied 2D linear and angular measures in an attempt to better define structures in 3D space. While these efforts provided new insight into orthodontic and surgical imaging, they fell short of fully utilizing the 3D potential of CBCT and appreciating true anatomical form. Through the establishment of 3D averages of the Korean adult normative skulls, this study demonstrated the potential for creating multiple sub-normative skull averages with respect to gender, ethnicity, age groups, and other unique characteristics. The ability to compare an individual's surface map and boundary to a specific sub-normative model yields more detailed deviation and dysmorphology than the information produced by comparing it to a generalized norm. Additionally, a combination of colorized linear, vector, and statistical maps will prove particularly useful in cases with notable

asymmetries, craniofacial anomalies, or extreme growth patterns in which visual inspection and 2-dimensional analyses alone is inadequate. As the field of orthodontics continues to advance and the usage of 3D CBCT increases, these key features will provide a stepping-stone to a true 3D analysis and an avenue for further 3D studies to advance our field.

Furthermore, development of such sub-normative skull models opens doors beyond the field of orthodontics and can be applied to anthropologic and genetic sciences. For example, anthropologists conduct complex and time-consuming morphometric analyses of human populations to better understand anatomical variations within and among different groups. The ability to produce population-based or geographic-based atlases of the human skull may offer one more tool in their quest to better understand human evolution and development.

4.2 Limitations

As this project provides a foundation for establishing various sub-normative skulls in the long term, the biggest limitation is gathering normative data that fit our stringent inclusion and exclusion criteria mentioned in the Materials and Methods section. We define 'norm' as a widespread standard typical in a large group; however, prospective orthodontic patients that require CBCT for diagnosis typically present with impacted teeth, skeletal asymmetry or discrepancy that require surgical intervention, or complex problems. Thus, there is a challenge of having acquiring CBCT scans for skeletal class I patients. Through our collaboration with Dr. Sujung Kim from Kyung Hee University in Korea, we were able to obtain a small number of samples to derive our norms. Moving

forward, we are optimistic that further collaboration with other institutions domestically and internationally will help us gather a large amount of data to derive sub-normative skulls.

Another limiting factor was the variability in image resolution of CBCT scans, soft tissue noise, and bone thickness in certain areas. Although we used the same CBCT machine – Alphard 3030 Model 3D X-ray CT Scanner – for all our samples, the surface definition in regions such as the nasal bone and anterior nasal spine were not well defined during hard tissue optimization and surface segmentation. We believe that the improvement in imaging quality and CBCT technology will eventually overcome this problem in the future.

Furthermore, there is a lack of semi-automation in extraction of boundary information with the current protocol. Currently, the manual digitization along the boundaries of the maxilla, cranial base, and mandible is required, a time and labor consuming process. Thus, we are in the process of developing a protocol for semi-automating the digitization process to make it more user-friendly, efficient, and less time-consuming.

Lastly, there are six different developed pipelines that need to be run in order to arrive at our result. With this many pipelines, it is easy for a user to make a mistake of inputting a wrong parameter, and render incorrect statistical values or results. Therefore, we are working towards creating one master pipeline to make it more user friendly and less error-prone.

5. Conclusion

1. This study developed the protocol necessary to average the human skull utilizing surface mapping and a boundary analysis approach.
2. 11 Korean adult males and 13 Korean adult females with skeletal diagnosis of Class I and no previous history of orthodontics were successfully averaged using 7-parameter Procrustes alignment, producing respective sub-normative skulls.
3. Internal and external sample patient skulls were superimposed on the respective sub-norm, creating a colorized displacement map, vector map, and statistical map, and illustrating potential clinical utility in diagnosis and treatment planning of patients with complex skeletal conditions.
4. Further research efforts will focus on gathering more samples to derive different sub-norms with respect to ethnicity, age, gender, and other unique characteristics. In addition, we will attempt to integrate the protocol described here and soft tissue averaging protocol to develop a comprehensive analysis of a given patient.

References

1. American Academy of Oral and Maxillofacial Radiology, 'Clinical Recommendations Regarding Use of Cone Beam Computed Tomography in Orthodontics. Position Statement by the American Academy of Oral and Maxillofacial Radiology.' *OOOO*, **116**, 238-57 (2013).

2. Proffit, W. *Contemporary Orthodontics*, 4th ed. Mosby Elselvier, 2007.

3. Broadbent, HB. A New X-ray Technique and its Application to Orthodontia. *The Angle Orthodontist*, 2009

4. Gleis, R., Brezniak, N., Lieberman, M. Israeli Cephalometric Standards Compared to Downs and Steiner Analyses. *The Angle Orthodontist*, **60**, 35–40; discussion 41 (1990).

5. Nanda, R., Nanda, R. S. Cephalometric Study of the Dentofacial Complex of North Indians.* *The Angle Orthodontist*. (1969).

6. Altemus, L. A Comparison of Cephalofacial Relationships. *The Angle Orthodontist*, **30**, 223-240 (1960).

7. Adams, G. Comparison between Traditional 2-Dimensional Cephalometry and a 3-Dimensional Approach on Human Dry Skulls. *AJODO*, **126**, 397-409 (2004).

8. Naragond, A., Kenganal, S. Diagnostic Limitations of Cephalometrics in Orthodontics - A Review. *IOSR Journal of Dental and Medical Sciences*, **3**, 30-35 (2012).

9. Steiner, C. C. The Use of Cephalometrics as an Aid to Planning and Assessing Orthodontic Treatment: Report of a Case. *American Journal of Orthodontics*, **46**, 721-35 (1960).

10. Agrawal, D. Cephalometric Analysis for Diagnosis and Treatment of Orthodontic Patients. Orthodontic Cyber Journal. (2012).

11. Kapila, S., Conley, R. S. & Harrell, W. E. The current status of cone beam computed tomography imaging in orthodontics. *Dentomaxillofacial Radiol.* **40,** 24–34 (2011).

12. Ghoneima, A., Allam, E. 'Three-Dimensional Imaging and Software Advances in Orthodontics' in *Orthodontics - Basic Aspects and Clinical Considerations*, ed. by Farid Bourzgui. InTech (2012).

13. Machado, G. L. CBCT Imaging – A Boon to Orthodontics. *The Saudi Dental Journal*, **27**, 12-21 (2015).

14. Harrell, W. E., Hatcher, D. C., Bolt, R. L. In search of anatomic truth: 3-dimensional digital modeling and the future of orthodontics. *AJODO,* **122,** 325–330 (2002).

15. Koltai, P. J., Wood, G. W. Three dimensional CT reconstruction for the evaluation and surgical planning of facial fractures. *Otolaryngol.--Head Neck Surg. Off. J. Am. Acad. Otolaryngol.-Head Neck Surg,* **95,** 10–15 (1986).

16. Girod, S., Keeve, E., Girod, B. Advances in interactive craniofacial surgery planning by 3D simulation and visualization. *Int. J. Oral Maxillofac. Surg.* **24,** 120–125 (1995).

17. Haffner, C. L., Pessa, J. E., Zadoo, V. P., Garza, J. R. A technique for three-dimensional cephalometric analysis as an aid in evaluating changes in the craniofacial skeleton. The *Angle Orthodontist.* (2009).

18. Ludlow, J. B., Gubler, M., Cevidanes, L., Mol, A. Precision of cephalometric landmark identification: Cone-beam computed tomography vs conventional cephalometric views. AJODO*,* **136,** 312.e1–313 (2009).

19. Bassan, B. *et al.* Precision of identifying cephalometric landmarks with cone beam computed tomography in vivo. *Eur. J. Orthod.* **35,** 38–44 (2013).

20. Cho, H. J. A Three-Dimensional Cephalometric Analysis. *J. Clin Orthod.* **XLIII,** 235–252 (2009).

21. Park, S.-H., Yu, H.-S., Kim, K.-D., Lee, K.-J., Baik, H.-S. A proposal for a new analysis of craniofacial morphology by 3-dimensional computed tomography. *AJODO,* **129,** 600.e23–600.e34 (2006).

22. Bayome, M., Park, J. H. & Kook, Y.-A. New three-dimensional cephalometric analyses among adults with a skeletal Class I pattern and normal occlusion. *Korean J. Orthod.* **43,** 62 (2013).

23. McComb, R. W. An Exploratory Approach for Mapping the Surface of the Human Skull in Three Dimensions: Technical Methods and Clinical Application. (2013). at <http://escholarship.org/uc/item/5gn4x0r2>.

24. Khullar, R., Lestrel, P. E., Moon, W., Wolfe, C. Representation of the Mandible as a Curve in 3-space: A Preliminary Study using Fourier Descriptors. World Scientific, 107–139 (2013).

25. Sung, J. 3-Dimensional Morphologic Analysis of the Craniofacial Skeletal Complex Using Geometry-Based Superimposition and Normalization. (2013).

26. Thompson, P. M. et al. Mapping Hippocampal and Ventricular Change in Alzheimer Disease. *NeuroImage*, **22**, 1754-1766 (2004).

27. Shi, Y. Inverse-Consistent Surface Mapping with Lapace-Beltrami Eigen-Features. *Inf Process Med Imaging*, **21**, 476-78 (2009).

28. Fischl, B., Sereno, M. I., Tootell, R. B., Dale, A. M. High-Resolution Intersubject Averaging and a Coordinate System for the Cortical Surface. *Human Brain Mapping*, **8**, 272-284 (1999).

29. Brechbuhler, C., Gerig, G., Kubler, O. Parametrization of Closed Surfaces for 3-D Shape Description. *Comput. Vis. Image Underst.*, **61**, 154-170 (1995)

30. Healy, D. M., Kostelec, P. J., Moore, S. B. FFTs for the 2-Sphere - Improvements and Variations. *The Journal of Fourier Analysis and Applications*, **9**, 341-385 (1996).

31. Everson, R. Orthogonal, but Not Orthonormal, Procrustes Problems. *Advances in Computational Mathematics* (1997).